Pure and Applied Geophysics

Seismic noise-based strategies for emphasizing the recent tectonic activity of blind thrusts: the case of the Ferrara Arc, Northern Italy

--Manuscript Draft--

Manuscript Number:	PAAG-D-18-00334
Full Title:	Seismic noise-based strategies for emphasizing the recent tectonic activity of blind thrusts: the case of the Ferrara Arc, Northern Italy
Article Type:	Regular Issue
Keywords:	seismotectonics; microtremors; ESAC; HVSR; OpenHVSR
Corresponding Author:	Riccardo Caputo Universita degli Studi di Ferrara Ferrara, ITALY
Corresponding Author Secondary Information:	
Corresponding Author's Institution:	Universita degli Studi di Ferrara
Corresponding Author's Secondary Institution:	
First Author:	Riccardo Caputo
First Author Secondary Information:	
Order of Authors:	Riccardo Caputo
	Ambra Mantovani
	Nasser Abu-Zeid
	Samuel Bignardi
	Gabriele Tarabusi
	Giovanni Santarato
Order of Authors Secondary Information:	
Funding Information:	
Abstract:	During the seismic crisis of May-June 2012, that strongly affected the central sector of the Ferrara Arc, relevant coseismic effects were observed, such as ground deformations and amplification phenomena due to low quality mechanical characteristics of the shallow subsurface (i.e. few hundreds of meters). This portion of the subsurface is not investigated by neither hydrocarbon explorations nor geotechnical surveys. Furthermore, direct analysis are not cost effective to carry out over such wide area. To overcome these limitations, we exploited seismic noise-based strategies, which are not invasive and don't require expensive equipments. We carried out several single-station and array measurements (i.e. HVSR and ESAC), across some of the major tectonic structures of the eastern Po Plain, belonging to the most advanced buried sector of the Northern Apennines. Such investigations were performed along two profiles, about 27 km-long and oriented SSW-NNE, i.e. almost perpendicular to the regional trend of the Ferrara Arc structures. Our results clearly document lateral shear wave velocity variations and the occurrence of resonance phenomena between 0.52 and 0.85 Hz. Additionally, based on inversion procedures, we were able to infer the depth of the resonant interface(s) and we associated such interface(s) to the major known stratigraphic discontinuities, thus emphasizing the recent tectonic activity of the blind thrusts affecting this sector of the Ferrara Arc.
Suggested Reviewers:	Philippos Vallianatos Prof. of geophysics, University of Crete fvallian@chania.teicrete.gr moving at Athens University

	Dario Albarello Prof., Universita degli Studi di Siena Dipartimento di Scienze Fisiche della Terra e dell' Ambiente dario.albarello@unisi.it
	Barbara Dietiker, Dr geophysicist, Natural Resources Canada Earth Sciences barbara.dietiker@canada.ca
	Marijan Herak Prof. of geophysics, University of Zagreb herak@irb.hr
	Efthimios Sokos Prof. of Seismology, University of Patras esokos@upatras.gr

Seismic noise-based strategies for emphasizing the recent tectonic activity of blind thrusts: the case of the Ferrara Arc, Northern Italy

Mantovani A.[1,2], Abu Zeid N.[1,2], Bignardi S.[1,2,3] Tarabusi G.[4], Santarato G.[1,2], Caputo R.[1,2,5]

1) Dept. Physics and Earth Sciences, via Saragat 1, Ferrara
2) Centro interuniversitario per la ricerca sismotettonica, CRUST-UniFE, Italy
3) School of Electrical and Computer Engineering, Georgia Institute of Technology, Georgia, USA
4) Istituto Nazionale di Geofisica e Vulcanologia, Roma, Italy
5) Research and Teaching Center for Earthquake Geology, Tyrnavos, Greece

Abstract

During the seismic crisis of May-June 2012, that strongly affected the central sector of the Ferrara Arc, relevant coseismic effects were observed, such as ground deformations and amplification phenomena due to low quality mechanical characteristics of the shallow subsurface (*i.e.* few hundreds of meters). This portion of the subsurface is not investigated by neither hydrocarbon explorations nor geotechnical surveys. Furthermore, direct analysis are not cost effective to carry out over such wide area. To overcome these limitations, we exploited seismic noise-based strategies, which are not invasive and don't require expensive equipments. We carried out several single-station and array measurements (*i.e.* HVSR and ESAC), across some of the major tectonic structures of the eastern Po Plain, belonging to the most advanced buried sector of the Northern Apennines. Such investigations were performed along two profiles, about 27 km-long and oriented SSW-NNE, *i.e.* almost perpendicular to the regional trend of the Ferrara Arc structures. Our results clearly document lateral shear wave velocity variations and the occurrence of resonance phenomena between 0.52 and 0.85 Hz. Additionally, based on inversion procedures, we were able to infer the depth of the resonant

interface(s) and we associated such interface(s) to the major known stratigraphic discontinuities, thus emphasizing the recent tectonic activity of the blind thrusts affecting this sector of the Ferrara Arc.

keywords: seismotectonics; microtremors; ESAC; HVSR; OpenHVSR

Introduction

The Po Plain is one of the most densely populated areas worldwide, because of the favorable combination of morphological, hydrological, climatic factors, and availability of natural resources, which make this, as well as most of the alluvial plains advantageous for the human settlements. Considering the amount of human and infrastructures exposure of the Po Plain associated with its seismogenic potential, it is clear that the seismic risk is particularly high.

The area we investigated pertains to the central-eastern sector of the Po alluvial Plain, which represents the foredeep of two opposite-verging fold and thrust belts, the Northern Apennines and the Southern Alps. In particular, we focused on the shallowest portion (down to few hundreds of meters) of the Ferrara Arc (Figure 1), which is one of the three major blind arcs, consisting of mainly north-verging thrusts and asymmetric folds forming the external front of the Northern Apennines. Despite its flat topography, past hydrocarbon exploration (Pieri & Groppi, 1981) revealed that the external thrusts of the Apennines have fairly irregular shape and are covered by a variable thickness of clastic Pliocene-Quaternary materials (GeoMol Team, 2015).

As it is common in large and tectonically active continental foredeep basins, the Po Plain is characterized by blind faulting (Vannoli *et al.*, 2014). Blind faulting became widely debated in the Earth Sciences community in the 80’s, when a series of ‘hidden earthquakes’ hit the central and southern California (1983-1987), and subsequently culminated with the Loma Prieta earthquake in 1989 (Burrato *et al.*, 2012).

Several authors hypothesized that the tectonic activity of the frontal part of the Northern Apennines ceased in the early Pleistocene (Argnani and Frugoni, 1997; Bertotti *et al.*, 1998; Argnani *et al.*, 2003; Picotti and Pazzaglia, 2008); while other studies, based on geomorphological and cinematic indicators, suggest that some of the anticlinal structures buried below the Po Plain may still be tectonically active (Burrato *et al.*, 2003; Boccaletti *et al.*, 2004; 2011; Scrocca *et al.*, 2007).

The latter hypothesis was clearly confirmed by the seismic sequence that affected the eastern sector of the Po Plain on May 20 and 29, 2012 (M_w = 6.1 and 5.9, Pondrelli *et al.*, 2012), causing 27 casualties, thousands of injuries, and severe damages, both to historical centers and industrial areas. Besides the relevant social, cultural, emotional and economic impacts, this sequence promoted a new interest about the dynamic properties of the shallow subsurface, especially in connection to the on-going microzoning studies in those areas where site effects were particularly severe (Priolo *et al.*, 2012; Martelli and Romani, 2013).

Considering the pressing necessity of characterizing vast areas from the dynamic point of view, the present work focuses on the determination of both the shear-wave velocity distribution and the fundamental resonance frequency of shear waves along two ca. 27 km-long profiles, that perpendicularly cross the Ferrara Arc tectonic system, using passive seismic methods. One major purpose of this research is to improve the knowledge of the geophysical properties of the shallow subsurface through the investigation of the distribution of the elastic properties (down to one to two hundreds of meters), as they play a key role in controlling specific site effects, such as amplification/de-amplification of the seismic-signals, liquefaction, settlement, induced landslides, etc. Further, the lateral variations of such geophysical properties, captured trough the investigation of the propagating wavefield (Bignardi *et al.*, 2013; 2014), represent the perfect tool for inferring the recent tectonic evolution of this sector of the Po Plain (Tarabusi and Caputo, 2016).

The assessment of the “regional” seismic hazard is not sufficient for the definition of the seismic action in similar seismotectonic contexts, where a thick sedimentary cover is present., Indeed, the regional seismic hazard provides an evaluation of ground shaking for rock or stiff soil conditions (*i.e.* the so-called seismic bedrock) which can be strongly altered by local effects, both in terms of peak values, duration, and frequency content (Boatwright *et al.*, 1991; Caserta *et al.*, 1999; Margheriti *et al.*, 2000).Such phenomenon was clearly observed during the May 2012 Emilia seismic sequence (Bordoni *et al.*, 2012).

The need of a reliable strategy for the assessment of the site amplification led to the development of several techniques capable of identifying the main characteristics of site response due to the presence of soft deposits. The approaches based on numerical simulation coupled with dedicated geophysical and geotechnical surveys (penetrometric tests, cross-hole, borehole, etc.) suffer from severe limitations in urbanized areas because of the elevate cost and site accessibility issues. Alternative techniques use earthquake recordings to experimentally estimate the site response and therefore, provide an unbiased estimation of the amplification factor. Although the latter approach is the most reliable, its application is impractical in areas with low seismicity rates (Bonnefoy-Claudet *et al.*, 2006). In general, in the context of site amplification studies a key role is played by the shear-wave velocity (V_S). Indeed, the Vs is directly related to the resistance of subsurface materials to shear forces (Okada, 1986; Ohori *et al.*, 2002) and it is therefore important for their quantitative evaluation. Estimating V_S in-situ through direct investigation is impractical because of the realization costs and the limited depth of investigation (generally around 30 m). Therefore, the application of low-cost and non-invasive techniques, although indirect, becomes particularly attractive, especially when large areas have to be investigated.

Since the pioneer work of Kanai *et al.* (1954), the seismic ambient noise became a widely used tool for the estimation of the seismic site response and for inferring the dynamical properties of the subsurface, especially when incoherent sediments are present. The development of new generation cost-effective digital seismographs resulted in the widespread use of portable instruments, as opposed to the fixed stations traditionally used for microzoning studies. Nowadays, two seismic noise-based strategies are routinely used to determine site response parameters: the single-station Horizontal to Vertical Spectral Ratio (Nogoshi and Igarashi 1970; HVSR; *e.g.* Nakamura, 1989) and the more advanced array techniques (*e.g.*, Refraction Microtremors - ReMi; Louie, 2001; Spatial AutoCorrelation - SPAC: Aki, 1957; 1964; Extended Spatial AutoCorrelation - ESAC: Ohori *et al.*, 2002; Okada, 2003).

We used the afore-mentioned techniques at sparse locations, so to cover the entire territory under investigation. In particular, as mentioned above, we used such techniques in order to gain insight on the shear wave velocity variation in the shallow subsurface as well as on the fundamental resonance frequency, and we focused on two transects, 27 km-long, crossing the central sector of the Ferrara Arc in SW-NE direction, almost perpendicular to the regional trend of the buried structures. The collected data were used to reconstruct pseudo-2D sections of the shallow sedimentary cover, nearly down to 160-180 m, so emphasizing the occurrence of lateral shear wave velocity and fundamental frequency variations, which reflect analogous stratigraphic changes that could be interpreted to be a consequence of the Late Quaternary tectonic evolution. Additionally, in order to investigate the presence of deep discontinuities, in terms of surfaces of major elastic impedance contrast, the obtained shear wave velocity profiles have been used as input start models for the inversion of the HVSR curves.

Geological and geodynamic framework of the Po Plain

The Po Plain represents the widest nearly flat area of Italy, extending for over 400 km in an approximately E-W direction from the western Alps to the Adriatic Sea, and it corresponds to the drainage basin of the Po River and its tributaries. Its morphological boundaries are represented by the contact between the Quaternary alluvium outcropping in the plain, the Southern Alps to the north and the exposed portion of the Northern Apennines to the south.

The structural setting of the Po Plain was imaged for the first time during the past decades by a dense grid of reflection seismic profiles in the frame of hydrocarbon and water resources explorations (AGIP Mineraria, 1959; AQUATER, 1976; 1978; AQUATER-ENEL, 1981). The most impressive features of the Po Plain are buried beneath a thick syntectonic succession, deposited in the Neogene-Quaternary foredeep (Figure 1). This configuration is the result of the combination of fast subsidence-sedimentary rates and conversely low tectonic activity, resulted in the complete sealing of the external fronts of the Northern Apennines. Indeed, the real fold-and-thrust belt front is located in the central-southern portion of the Po Plain made of four major blind arcs: the Monferrato Arc, the Emilia Arc, the Ferrara Arc and the Adriatic Arc (Castellarin *et al.*, 1985). In particular, the Ferrara Arc started to develop in early Pliocene (Costa, 2003; AQUATER, 1978, 1980; in middle-late Pliocene, according to Patacca and Scandone, 1989), nowadays it runs from Reggio Emilia town to the Adriatic Sea and Marche coastal sector and consists of Messinian-Quaternary autochthonous and parautochthonous, terrigenous deposits overlying Mesozoic to Palaeogene carbonate units (Pieri and Groppi, 1981; Nardon *et al.*, 1991). The outer border of this arc is marked by a set of structural highs originated by fault-propagation folds arranged roughly en-echelon (*e.g.*, Pieri and Groppi, 1981), where the thickness of the Quaternary succession is locally only 100 m or less (Paolucci *et al.*, 2015; Tarabusi and Caputo, 2016). In contrast, the inner and outer portions of the arc are depressed and covered by a Quaternary sequence thicker than 800 m.

The architecture of the Po Plain foredeep filling, from Pleistocene onward, is characterized by a generally regressive trend, interrupted by smaller fluctuations, evidenced by the transition from offshore Pliocene deposits to marine-marginal and then to alluvial Quaternary sediments (Ricci Lucchi, 1986; Amorosi and Colalongo, 2005; Amorosi, 2008).

The great number of subsurface data collected during hydrocarbon explorations and water research (AGIP Mineraria, 1959; AQUATER, 1976, 1978; AQUATER-ENEL, 1981; Pieri & Groppi, 1981; RER & ENI-AGIP, 1998; Boccaletti *et al.*, 2004, 2011; Molinari *et al.*, 2007) allowed to map the main Quaternary unconformities too; at the regional scale the most recent of such surfaces represents the base of the Upper Emiliano-Romagnolo Synthem (AES; Boccaletti *et al.*, 2004) which consists of a series of different depositional cycles whose limits are placed in correspondence of the bottom of the transgressive marine deposits. The transgressive portion of each cycle is characterized by the presence of fine materials (*e.g.* floodplain, marsh and coastal plain clays) with subordinated sandy intercalations. Instead, the regressive sequence consists of alluvial plain deposits (*e.g.* fine sediments of overflowing river) where channel sands are subordinated in the form of isolated lenticular bodies. On top of each cycle, the channel sands become abundant, thus forming laterally wider bodies (RER & ENI-AGIP, 1998; ISPRA, 2009).

Several studies reveal that the Quaternary succession is highly deformed and confirm that the transitions from marine to continental sediments coincide with important tectonic phases followed by periods of strong subsidence (RER & ENI-AGIP, 1998; Boccaletti *et al.*, 2004; 2011; Abu Zeid *et al.*, 2013; 2014; Martelli and Romani, 2013; Molinari *et al.*, 2007; Paolucci *et al.*, 2015; Tarabusi and Caputo, 2016). Therefore, the highly variable thickness of the Quaternary sequence from several hundreds in the synclines to few tens of meters in correspondence of the growing anticlines, like those named Mirandola, Casaglia and Argenta, reflects the influence of the complex evolution of the blind thrusts belonging to the Ferrara Arc.

Geophysical noise-based methods

As above mentioned, both invasive and non-invasive geophysical methods are routinely employed in seismic hazard and microzoning studies (*e.g.* Martelli and Romani, 2013; and, as an example of invasive and non-invasive methods comparison in the Emilian area, see Garofalo *et al.* 2016a; 2016b). The choice between the most effective investigation method depends on lithology, desired investigation depth, and free space available at the surface In general, whenever conditions are favorable, geophysical methods provide a faster and low-cost way, as compared to direct methods (Lai *et al.*, 2000).

Capturing the distribution of V_S in the subsurface is nowadays obtained by inverting the dispersion spectrum of surface waves Rayleigh and Love recorded on a multi-channel seismogram using low frequency vertical and horizontal geophones respectively. Active (MASW: Park *et al.*, 1999) and passive (Re.Mi., SPAC, ESAC: see below) approaches are equally diffused. In MASW, the investigation depth, a part of profile length, is tightly bound to the strength of the seismic source, signal-to-ambient noise ratio, and signal attenuation, therefore it is generally impractical for depths greater than 30-50 m. As the ambient noise lies in the law frequency range (*i.e.* long wavelengts) passive, noise-based methods does not suffer such a limitation and the investigation depth mostly depends on the width of the geophone array.

In this paper, to reconstruct geophysical pseudo-2D sections along two transects, several kilometers-long, crossing the central sector of the Ferrara Arc (A-A' and B-B' in Figure 1), two seismic noise-based methods were employed, *i.e.* ESAC and HVSR.

The seismic ambient noise (hereafter ‘noise’) is a set of small amplitude oscillations (10^{-4}-10^{-2} mm) of the ground materials characterized by a wide frequency content (0.05-100 Hz), partially below human sensing originated by a number of different natural sources such as wind, oceanic waves and meteorological conditions (*i.e.* microseisms) or of artificial origin such as road traffic, trains, and industrial activitie (*i.e.* microtremors; Gutenberg, 1958; Asten, 1978; Asten and Henstridge, 1984).

As of 1950s, diffusion of seismology and of related technical improvements allowed significant advances in the understanding of noise phenomena. Several authors investigated the origin and the nature of noise as well as the possible noise-based techniques and applications. One of them is based on an array of sensors, laid out along a linear profile (Re.Mi.: Louie, 2001), or a circle (SPAC; Aki, 1957; 1964) or along T, L, or X-shaped distribution of geophones (ESAC: Ohori *et al.*, 2002, Okada, 2003), and thus, conceptually, on wave time delay measurements between coupled stations. These methods are linked with the property of surface waves dispersion can be used to obtain the vertical shear-wave velocity profile. There are two main techniques to process the array datasets: the frequency-wave number analysis (f-k; Capon *et al.*, 1967; Capon, 1969; Lacoss *et al.*, 1969) and the spatial autocorrelation analysis (SPAC; Aki, 1957; 1964).

The use of single-station noise recordings for the estimation of the local site effects has become increasingly popular, especially thanks to its simple approach which requires the use of a single three-component seismograph and its applicability also in areas of low or even no observed or registered seismicity; moreover it is nowadays enhanced by a wide range of low cost instruments. The HVSR technique was firstly proposed by Nogoshi and Igarashi (1970), and became popular thanks to Nakamura (1989) who intended to estimate the relative amplification or deamplification level due to the incidence of S-waves at the base of soft sediments by means of spectral analysis of microtremor measurements. In this way he argued that this technique is capable of deriving the fundamental resonance frequency of a site, while real amplification levels can't be correctly estimated and still more research is needed to be done (Bard, 1999; SESAME, 2004). Among the several applications of the Nakamura technique, which span a variety of scientific disciplines, such as geology (Mantovani *et al.*, 2018), seismology and microzonation studies (Scherbaum *et al.*, 2003; Gallipoli *et al.*, 2004, Massolino *et al.*, 2018) and even archaeology (Obradovic *et al.*, 2015, Abu Zeid *et al.*, 2016; 2017), one of the most attractive is the estimation of the depth of the major impedance contrasts (*i.e.* in most cases the depth of the bedrock) through dedicated inversion procedures. The availability of fast and efficient modelling strategies favored the implementation of algorithms for the inversion of such curves, as for example the commercial software Grilla® (www.moho.world) or the open source Geopsy (http://geopsy.org). In 2008 Herak published a user friendly program in Matlab capable of obtaining the 1D distribution of the elastic properties of a subsurface consisting of a stack of layers by inverting a single HVSR curve, and later, Bignardi *et al.* (2016, 2018) published a set of programs dedicated to the processing and inversion of sparsely distributed microtremor measurements (https://github.com/sedysen/OpenHVSR).

Data collection and processing

Numerous array and single station noise measurements were performed along two profiles running from Cento to Bondeno (western Ferrara Province; A-A'; Figure 2a) and from Traghetto to Formignana (eastern Ferrara Province; B-B'; Figure 2b). Both profiles ca. 27 km-long and oriented SSW-NNE, andn almost perpendicular to the regional trend of the buried structures belonging to the Ferrara Arc.

Along the western profile, 7 Re.Mi. and 13 ESAC measurements were performed in 2012 and 2013, respectively, while in 2014, 26 ESAC were acquired along the eastern-most profile (Abu Zeid *et al.*, 2013; 2014) (Figure 2b). The measurement transects were selected in order to highlight possible strong lateral lithological variations (*i.e.* in terms of elastic properties); the average spatial sampling was around 1 km for both transects. Details about these measurements are summarized in Tables 1 and 2, respectively.

In order to carry out the ESAC measurements, L-shaped arrays, composed of 24 3-component low frequency geophones (4.5 Hz), 8 m-spaced, were laid out at each site. Data were recorded using an in-house made digital seismograph that allowed the continuous recording of time series with length ranging from 5 to 15 min and sampled at 500 Hz. The resulting mean array aperture of about 130 m allowed investigating the subsurface down to approximately 150-160 m depth.

Re.Mi. profiles were acquired using the RAS-24 digital seismograph by Seistronix (U.S.A.).. The processing of the array data was performed with the SeisOpt^R ReMi™ Software (http://www.optimsoftware.com/index.php/seisopt-remi-byoptim-software).

The single-station noise measurements were performed using a 3-component short-period seismometer, with 2 Hz proper frequency, connected a portable seismograph (Vibralog model, MAE srl, Italy, www.mae-srl.it). Following the SESAME Guidelines (SESAME, 2004) and since the resonance frequency was expected below 1 Hz, the minimum acquisition time was set to 30 minutes, at 250 Hz sampling rate. The seismometer was placed in a small hole filled with sand to insure easy levelling, good coupling and prevent any turbulence due to wind flowing around the seismometer (SESAME, 2004; Mucciarelli *et al.*, 2005). Along the eastern transect 21 ambient noise measurements were performed between June and October 2014, while for the western transects 16 measurements were carried out from October 2014 to May 2015. The average spatial sampling was around 1.2 km for the first transect, while we adopted an average spacing of 1.6 km for the second (Figure 2a,b). Microtremors acquired were processed using the Grilla® software and results are summarized in Tables 3 and 4, respectively.

Considering the characteristics of the seismometer, the analysis was limited down to the 0.5 Hz and extended to 20 Hz maximum. Each record was then split into 60 s period non-overlapping windows, for which amplitude spectra were computed and then smoothed using the Konno and Ohmachi window using b=40 (Konno and Ohmachi, 1998). The final HVSR is the average of the horizontal components spectra (in terms of amplitude) divided by the vertical one computed for each window. In addition, a directional analysis was performed in 10° angular increments in order to test the isotropy of the signal.

Afterwards, the 0.5-5 Hz portion of all HVSR curves was inverted using the OpenHVSR code (Bignardi *et al.*, 2016) to infer the shear wave velocity model.

Discussion

Retrieved 1D shear velocity models have been projected along the profile traces and their discrete information were interpolated using a minimum curvature algorithm (Briggs, 1974), specifically selected in order to avoid false high/low velocity values connected to the large spatial distance between measurements as compared to the shallow depth, and to minimize surface curvature under the constraint of the surface experimental velocity values. This procedure allowed to reconstruct interpolated pseudo-2D velocity sections along the two transects. Although some 1D models locally reached higher depths, the reconstructed sections were limited at about 160 m. Absolute elevetions along the profiles range from 7.1 to 14.5 m a.s.l. and 0.2 to 4.4 m a.s.l., respectively.

Western transect

The shear wave velocity values (Table 3 and Figure 3b-c) range between 100-150 m/s, at very shallow depth, and 500 m/s, at the maximum depth in correspondence of the central-northern portion of the profile. The vertical V_S gradient is observed to be strong between ReMi009-ESAC003 and ESAC010-ESAC013. In contrast, this gradient is weaker in the central sector of the profile, between ReMi010 and ESAC001, where maximum obtained V_S values, at 160 m b.s.l., is around 400 m/s. In a recently published paper, Minarelli *et al.* (2016), based on downhole Vp and Vs measurements performed in a well located between Mirabello and San Carlo villages, not too far from our investigated transect, confirmed a measured shear wave velocity of +/- 400 m/s between 100 to 240 m depth, which is in excellent agreement with our estimation.

Inversion of HVSR curves require a preliminary careful qualitative analysis of the microtremor characteristics, including peak clarity and stability for at least 10 or more time windows. When the peak is clear (and is not related to the anthropogenic activity), it indicates the presence of an acoustic impedance contrast at some depth and the peak frequency represents the natural frequency (f_0) of the site. If the thickness is known, an approximate estimation of the shear wave velocity can be obtained. On the contrary, if the curve is flat (HVSR average around 1), it is likely that the local velocity structure has no clear impedance contrasts (SESAME, 2004).

In Figure 4, a pseudo-2D section is shown as a function of frequency reconstructed using the HVSR profile routine (Herak *et al.*, 2010), which spatially interpolates the amplitude of the HVSR ratio obtained for each frequency bin. This section highlights the occurrence of an impedance contrast whose peak spatial evolution is associated to frequencies ranging from a minimum of 0.52 Hz up to a maximum of 0.79 Hz (Figure 4 and Table 3). The lowest fundamental resonance frequencies ($f_0 \leq 0.6$ Hz) are observed between sites 4 and 7, while, for the other sites f_0 is greater than 0.6 Hz. The HVSR amplitude (A_0) in the frequency section is color-coded and is systematically greater than 2.0. The largest values ($A_0 \geq 3.5$) are observed between sites 36 to 39, in the northern portion of the profile.

Assuming that the observed lateral variation of V_S (Figure 3a), f_0 and A_0 (Figure 4) do reflect lateral litho-chronological variations, especially in terms of differential compaction (*i.e.* age) of the sediments, the two pseudo-2D sections suggest the occurrence of buried anticlinal structures associated with a 'condensed' stratigraphy sequence and, taking into account the shallow depth investigated, their recent tectonic evolution (for a similar correlation in the Mirandola area see Tarabusi and Caputo, 2016).

Nowadays, the strategy behind a 2D HVSR investigation is through "HVSR-profiling" (Herak *et al.*, 2010), which consists of placing the different HVSR curves obtained along a linear profile, back to back and translating the frequency axis into "pseudo-depth" by means of some analytic or empirical relations (*e.g.* $f_0 = V_S/4h$ or alternatively using a power law where V_S smoothly increases with depth). Although these strategies contribute to a better understanding of the subsoil architecture, they do not provide any information about the elastic properties and impedance contrasts depths. This drawback is generally solved by comparing the pseudo-2D picture with 1D models obtained by inverting the HVSR curves at few key locations.

This issue has been tackled by Bignardi *et al.* (2016), by developing an open source program under Matlab environment, named OpenHVSR, for the simultaneous modeling and inversion of massive HVSR datasets, based on a guided Montecarlo approach. The forward modeling routine (FWD) implements the same modeling strategy proposed in ModelHVSR (Herak, 2008). OpenHVSR implements tools that make data management flexible and intuitive and help in reducing the time necessary for data inversion.

Using the OpenHVSR code, all the HVSR curves performed along the investigated profiles were inverted. The input values for V_P and V_S were provided by the ESAC inverted models. However, the ESAC and HVSR inversion processes are based on forward models with inherently different simulation approaches. Indeed, while the ESAC inversion is engineered to retrieve a smooth model, the latter is not suitable as initial model for the HVSR inversion. Indeed, in order to correctly reproduce the spectral ratio peaks, well defined acoustic impedance contrasts are required. For this reason, the smooth V_S subsurface model obtained from the ESAC was piecewise averaged to produce a blocky layered model to be used as a starting guess to initiate the HVSR inversion process. In this way, we obtained the advantage of starting from a model already residing in the “basin attraction” of the HVSR inversion global minima. Therefore, it was possible to optimize the local V_S profiles in order to minimize the HVSR objective functions. In order to perform the optimization of the subsurface and to reproduce the HVSR peaks a maximum perturbation of 5% of the elastic parameter (*i.e.* P-wave velocity, S-wave velocity, thickness, density, P-wave and S-wave frequency-dependent attenuation) was allowed for the first 5000 model generations, and successively, in order to enrich the space of parameters sampling, a 15% perturbation was allowed for the subsequent 25000.

In the following, a selected HVSR curve is shown as an example, and discussed to some detail. The selected curve pertains to the western profile (site 39; Figure 2a). The starting 8-layers blocky model (Figure 5a), in terms of thickness and body waves velocity, was derived from the smooth subsurface profile obtained from the ESAC investigation, and extracting the 1D profile at the closest location (*i.e.* ESAC013). Concerning density and attenuation factors, the values suggested by Laurenzano *et al.* (2013) for a nearby site where used. The visco-elastic parameters of bedrock, were kept fixed for all the locations. From one hand, it is well known (Herak, 2008) that the Vs value at bedrock can affect the amplitude of the spectral ratio, while leaving the location of the resonant peak almost unchanged. On the other hand, the true information of HVSR resides in the peak frequency location. We observed that a Vs value of 800 m/s (justified by considering a crosshole survey performed by the Regione Emilia-Romagna, close to the Casaglia cemetery; Di Capua and Tarabusi, 2013), was capable of reproducing the spectral ratio quite well. It should be noted however that the latter site is located in correspondence of the top of the Casaglia anticline where the real bedrock is certainly shallower than at site 39 and hence the velocity gradient stronger. Nevertheless, whether such a high value of Vs is actually justified for the whole area has recently been matter of discussion (Foti *et al.*, 2009). Therefore, in order to investigate this aspect and to keep consistent with the Vs values observed using ESAC, we performed few simulations and verified that even at lower Vs values, say as slow as 600 m/s, the overall position of the frequency peaks was not altered.

The final blocky layered subsurface model is shown in Figure 5b. The best fit between the experimental and theoretical HVSR curves and the comparison between the smoothed ESAC and the best HVSR blocky subsurface inversion are shown in Figures 5c and 5d, respectively. Moreover, theoretical dispersion curve calculated for the final model resulted very similar to the experimental dispersion curve obtained from the analysis of the ESAC013 profile (Figure 5e).

The results provided by the inversion of the HVSR curves, compared with the available geological information, show a good agreement with the major known stratigraphic unconformities (Figure 6). In particular, the shallower resonant interface represented in Figure 6a is likely associated with one of the Middle Pleistocene sedimentary cycles (Figure 6b) and specifically the AES6 (Complex Aquifer A2; RER and ENI-AGIP, 1998; Molinari *et al.*, 2007). This stratigraphic unit belongs to a higher rank sedimentary cycle represented by the Upper Emiliano-Romagnolo Synthem AES (RER and ENI-AGIP, 1998).

On the other hand, the deeper resonant interface (Figure 6a) may correspond to an older Middle Pleistocene unconformity (Figure 6b), namely the AESind (Complex Aquifer A4, RER and ENI-AGIP, 1998; Molinari *et al.*, 2007). According to the map of the bedrock depth proposed by Martelli and Romani (2013), this sedimentary interface has been considered as the seismic bedrock, although the Vs value associated to this stratigraphic unit (not much greater than 400 m/s) is lower than the values officially assumed for the “seismic bedrock” (EN 1998-5, 2004).

The geological section proposed by Martelli and Romani (2013) represented in Figure 6c clearly shows the occurrence of two buried anticline structures corresponding to the periclinal termination of the Mirandola anticline, to the south, and the Casaglia anticline, to the north. This geological setting strongly suggests that the shallow stratigraphic features documented in this paper and constrained by the lateral shear-waves variations could be also directly associated with the tectonic activity of the blind thrusts that were persisting throughout the whole Late Quaternary.

It is also noteworthy the comparison between the obtained V_S profile with the Structural Model of Italy (Bigi *et al.*, 1992; Figure 7). We indeed observe that the greatest V_S gradients in our profile occur in correspondence of some major thrust faults and particularly to the associated Mirandola (*i.e.* periclinal termination) and Casaglia blind anticlines to the south and north, respectively. In between, a tectonically "depressed" area can be inferred based on low V_S velocity gradients indicating the presence of less compacted sediments (Figure 7).

Eastern transect

The estimated shear wave velocity along the eastern transect (Figure 8a) was found to range between 100 and 150 m/s, at very shallow depth, and 500-550 m/s, at maximum depth reached below the southern and northern portion of the profile (Figure 8b). The vertical V_S gradient is observed to be strong between sites 3 to 14 and sites 23 to 26. In contrast, this gradient is weaker in the southern and central sectors of the profile, at sites 1 and 2 and from sites 13 to 21, where maximum obtained V_S values, at 160 m b.s.l., is around 400-450 m/s.

Analogously to the western transect, several HVSR stations were acquired along the same transect using both the same equipment and acquisition parameters. All the HVSR curves were inverted, using the V_P and V_S values provided by the ESAC investigation as a starting guess of the subsurface. The reconstructed pseudo-2D (frequency) section reveals the presence of an impedance contrast whose peaks are associated with frequencies ranging from a minimum of 0.58 Hz up to a maximum of 0.85 Hz (Table 4 and Figure 9). Low fundamental resonance frequencies (f_0 < 0.7 Hz) are observed at sites 6, 9 and 11, while, for the other sites f_0 is greater than 0.7 Hz. The corresponding HVSR amplitude (A_0) varies between 2.0 to 3.1 (Table 4).

The results provided by HVSR inversion were then compared with the available geological information consisting of three geological profiles crossing at high angle the investigated transect Figure 2b). They show a good agreement with the major known stratigraphic unconformities (Figure 9). Similar to the eastern transect, the shallower resonant interface that has been detected between 73 to 115 m depth (Figure 9a) could correspond to a surface located within the AES6 Middle Pleistocene sedimentary cycles (Complex Aquifer A2; RER and ENI-AGIP, 1998; Molinari *et al.*, 2007) as indicated in Figures 9b, c and d. However, the deeper interface, located between 172 to 180 m depth (Figure 9a), could correspond to a surface located within the AESind (Figure 9b) Middle Pleistocene sedimentary cycle (Complex Aquifer A4, RER and ENI-AGIP, 1998; Molinari *et al.*, 2007).

In this case, as well, the comparison of our results with the Structural Model of Italy (Bigi *et al.*, 1992) show a good fit between the lateral variation of V_S and particular, velocity gradients are higher in correspondence of some major thrust faults and associated anticlines, namely the Argenta structure to the south and the Ferrara structures to the north. In between and in the southernmost sector of the profile, two tectonically “depressed” areas can be inferred based on low V_S velocity gradients which indicates the presence of softer sediments.

Concluding remarks

The present study provides some insight on the dynamic properties of a portion of the eastern sector of the Po Plain and in particular of the central zone of the Ferrara Arc, responsible of the historical earthquakes that hit Ferrara in 1570 and Argenta in 1624 (I_0 = 7-8; Guidoboni *et al.*, 2018; Rovida *et al.*, 2016).

Due to the combination of a fast subsidence and sedimentary rate and conversely a relatively low tectonic activity, the thrusts developed within the Po Plain are all blind (Figure 7). Moreover, the highly variable thickness of the Quaternary sequence from several hundreds to few tens of meters in correspondence of the growing Mirandola, Casaglia, Ferrara, and Argenta anticlines, reflects the influence of the complex evolution of the blind thrusts belonging to the major Ferrara Arc.

In order to investigate the shallow subsurface, we purposely selected two 26-27 km-long transects oriented almost perpendicularly to the regional trend of the buried structures, investigating them through passive seismic methods (*i.e.* ESAC and HVSR). Based on numerous 1D measurements carried out along such transects it was possible to reconstruct pseudo-2D sections. By means of low-cost geophysical surveys (cost-effective equipment and very small teams), our approach allowed to confirm the recent tectonic activity of the buried structures underlying this sector of the Po Plain. In particular, assuming that the Vs and the fundamental resonance frequency patterns are determined by both vertical and lateral lithological variations, the reconstructed pseudo-2D sections document the occurrence of a reduced (*i.e.* condensed) stratigraphic succession in correspondence of the major anticline structures. This was also confirmed by the ‘constrained’ inversion of the HVSR curves, used to infer the depth(s) of reflectors corresponding to the observed frequency(ies) peaks that resulted to be linked to some major stratigraphic unconformities.

Beyond the geological and tectonic information obtained along the two transects, all the measured sites within this sector of the Po Plain show an almost homogeneous distribution of Vs in the shallowest tens of meters. This information is crucial in seismic microzoning studies because, while from one hand these low values quite uniformly characterize the Vs30 parameter (commonly used to evaluate the local amplification, *i.e.* the local expected PGA), on the other hand, this research clearly documents that at slightly greater depths, say between 30 and 150 m, the subsurface is in contrast, strongly differentiated, with undoubtedly different seismic responses at different sites. Accordingly, we suggest that the Vs30 approach commonly used in microzonation studies is too simplistic because it ignores the presence of deep discontinuities and may lead to underestimating the seismic hazard. The described methodology and the achieved results may reveal valuable in the estimation of the local site response, which is known to strongly depend on the careful evaluation of the shear wave velocity profile down to the seismic bedrock.

Acknowledgements

The study has benefited from funding provided by the Italian Presidenza del Consiglio dei Ministri – Dipartimento di Protezione Civile (DPC). The findings and conclusions in this article are those of the author(s) and do not necessarily represent DPC official opinion and policies.

References

Abu-Zeid, N., Bignardi, S., Caputo, R., Mantovani, A., Tarabusi, G., and Santarato, G. (2013). Acquisition of V_S profiles across the Casaglia anticline (Ferrara Arc). DPC-INGV-S1 Project, Final Report, pp. 42-46.

Abu-Zeid, N., Bignardi, S., Caputo, R., Mantovani, A., Tarabusi, G., and Santarato, G. (2014). Shear-wave velocity profiles across the Ferrara Arc: a contribution for assessing the recent activity of blind tectonic structures. In Proceedings of the 33th Conference of the National Group of Solid Earth Geophysics, volume 1, pages 117–122.

Abu Zeid, N., Corradini, E., Bignardi, S., Santarato, G., (2016) Unusual geophysical techniques in archaeology - HVSR and induced polarization, a case history, 22nd European Meeting of Environmental and Engineering Geophysics, NSAG-2016, DOI 10.3997/2214-4609.201602027.

Abu Zeid, N., Corradini, E., Bignardi, S., Nizzo, V., Santarato, G., (2017). The passive seismic technique 'HVSR' as a reconnaissance tool for mapping paleo-soils: the case of the Pilastri archaeological site, northern Italy, Archaeological Prospection, DOI 10.1002/arp.1568.

AGIP-MINERARIA (1959). Campi gassiferi padani. In Atti Convegno 'Giacimenti Gassiferi dell'Europa Occidentale'. Accademia Nazionale dei Lincei.

Aki, K. (1957). Space and time spectra of stationary stochastic waves, with special reference to microtremors. Bull. Earth. Res Inst., 35:415–456.

Aki, K. (1964). A note on the use of microseisms in determining the shallow structures of the earth's crust. Geophys., 29:665–666.

Albarello, D., Cesi, C., Eulili, V., Guerrini, F., Lunedei, E., Paolucci, E., Pileggi, D., and Puzzilli, L. (2011). The contribution of the ambient vibration prospecting in seismic microzoning: an example from the area damaged by the 26th April 2009 L'Aquila (Italy) earthquake. BGTA, 52(3):513–538.

Amorosi, A. and Colalongo, M. (2005). The linkage between alluvial and coeval nearshore marine succession: evidence from the Late Quaternary record of the Po River Plain, Italy. In: M. Blum and S. Marriott (Eds.) Fluvial Sedimentology, IAS Special Publication.

Amorosi, A. (2008). Delineating aquifer geometry whitin sequence stratigraphic framework: evidence from Quarnary of the Po River Basin Northern Italy. GeoActa Special Publication, 1:1–14. Bologna.

AQUATER (1976). Elaborazione dei dati geofisici relativi alla Dorsale Ferrarese. Rapporto inedito per ENEL.

AQUATER (1978). Interpretazione dei dati geofisici delle strutture plioceniche e Quaternarie della Pianura Padana e Veneta. Rapporto inedito per ENEL.

AQUATER (1980). Studio del nannoplancton calcareo per la datazione della scomparsa della Hyalinea baltica nella Pianura Padana e Veneta. Rapporto inedito per ENEL.

AQUATER-ENEL (1981). Elementi di neotettonica del territorio italiano. Volume speciale, Roma.

Argnani, A., Barbacini, G., Bernini, M., Camurri, F., Ghielmi, M., Papani, G., Rizzini, F., Rogledi, S., and Torelli, L. (2003). Gravity tectonics driven by Quaternary uplift in the Northern Apennines: insights from the La Spezia-Reggio Emilia Geo-Transect. Quat. Int., 101(102):13–26.

Argnani, A. and Frugoni, F. (1997). Foreland deformation in the Central Adriatic and its bearing on the evolution of the Northern Apennines. Ann. Geophys.

Asten, M.W. (1978). Geological control of the three-component spectra of Rayleigh-wave microseisms. BSSA, 68(6):1623–1636.

Asten, M. W. and Henstridge, J. D. (1984). Arrays estimators and the use of microseisms for reconnaissance of sedimentary basins. Geophys., 49(11):1828–1837.

Bard, P.-Y. (1999). Microtremor measurements: a tool for site estimation?, State-of-the-art paper, Second International Symposium on the Effects of Surface Geology on seismic motion, Yokohama, December 1-3, 1998, Irikura, Kudo, Okada & Sasatani (eds), Balkema 1999, 3, pp. 1251-1279.

Bertotti, G., Capozzi, R., and Picotti, V. (1998). Extension controls Quaternary tectonics, geomorphology and sedimentation of the N-Apennines foothills and adjacent Po Plain (Italy). Tectonophys., 282:291–301.

Bigi, G., Cosentino, D., Parotto, M., Sartori, R., and Scandone, P. (1992). Structural Model of Italy, scale1:500.000. 114(3). Prog. Fin. Geodinamica, Quad. 'La Ricerca Scientifica', C.N.R., Roma.

Bignardi, S., Fedele, F., Santarato, G., Yezzi, A., Rix, G., (2013). Surface Waves in Laterally Heterogeneous Media, Journal of Engineering Mechanics, 139(9), 1158-1165.

Bignardi, S., Santarato, G., Abu Zeid, N., (2014). Thickness Variations in Layered Subsurface Models – Effects on Simulated MASW, 76th EAGE Conference & Exhibition, Ext. abstract WS6¬P04. DOI 10.3997/2214-4609.20140540.

Bignardi S., Mantovani A. and Abu Zeid N., (2016). 'OpenHVSR: imaging the subsurface 2D/3D elastic properties through multiple HVSR modeling and inversion'. Computers & Geosciences, 93, 103-113.

Bignardi, S., 2017. The uncertainty of estimating the thickness of soft sediments with the HVSR method: A computational point of view on weak lateral variations. Journal of Applied Geophysics, 145C, 28-38, DOI 10.1016/j.jappgeo.2017.07.017.

Boatwright, J., Fletcher, J., and Fumal, T. (1991). A general inversion scheme for source, site and propagation characteristics using multiply recorded sets of moderate-sized earthquakes. BSSA, 81:1754–1782.

Boccaletti, M., Bonini, M., Corti, M., Gasperini, G., Martelli, L., Piccardi, L., Severi, P., and Vannucci, G. (2004). Carta sismotettonica della Regione Emilia-Romagna scala 1:250000. Note illustrative. A cura di M. Boccaletti e L. Martelli. S.EL.C.A, Firenze.

Boccaletti, M., Corti, G., and Martelli, L. (2011). Recent and active tectonics of the external zone of the Northern Apennines (Italy). Int. J. Earth Sci., 100:1331–1348.

Bonnefoy-Claudet, S., Cornou, C., Bard, P., Cotton, F., Moczo, P., Kristek, J., and Fäh, D. (2006). H/V ratio: a tool for site effects evaluation. Results from 1-D noise simulations. Geophys. J. Int., 167:827–837.

Bordoni, P., Azzara, R., Cara, F., Cogliano, R., Cultrera, G., Di Giulio, G., Fodarella, A., Milana, G., Pucillo, S., Riccio, G., Rovelli, A., Augliera, P., Luzi, L., Lovati, S., Massa, M., Pacor, F., Puglia, R., and Ameri, G. (2012). Preliminary results from EMERSITO, a rapid response network for site-effect studies. Ann. Geophys., 55(4):599–607.

Briggs, I.C. (1974). Machine contouring using minimum curvature: Geophysics, 39, 39-48.

Burrato, P., Ciucci, F., and Valensise, G. (2003). An inventory of river anomalies in the Po Plain, northern Italy: evidence for active blind thrust faulting. Ann. Geophys., 46(5):865–882.

Burrato, P., Vannoli, P., Fracassi, U., Basili, R., and Valensise, G. (2012). Is blind faulting truly invisible? Tectonic-controlled drainage evolution in the epicentral area of the May 2012, Emilia-Romagna earthquake sequence (northern Italy). Ann. Geophys., 55(4):525–531.

Capon, J., Greenfield, R. J., and Kolker, R. J. (1967). Multidimensional maximun-likehood processing of a large-aperture seismic array. IEEE, 55:192–211.

Capon, J. (1969). High-resolution frequency-wavenumber spectrum analysis. IEEE, 57:1408–1419.

Caserta, A., Zahradnik, J., and Plicka, V. (1999). Ground motion modeling with a stochastically perturbed excitation. J. Seismol., 3:45–59.

Castellarin, A., Eva, C., Giglia, G., Vai, G., Rabbi, E., Pini, G., and Crestana, G. (1985). Analisi strutturale del Fronte Appenninico Padano. Giornale di Geologia, 47:47-75.

Costa, M. (2003). The Buried, Apenninic Arcs of the Po Plain and Northern Adriatic Sea (italy): A New Model. Boll. Soc. Geol. It., 122:3–23.

Di Capua, G. and Tarabusi, G. (2013). Site specific hazard assessment in priority areas. DPC-INGV-S2 Project, Annex 3 to Deliverable 4.1.

EN 1998-5 (2004). Eurocode 8: Design of structures for earthquake resistance - Part 5: Foundations, retaining structures and geotechnical aspects, CEN European Committee for Standardization, Bruxelles, Belgium.

Foti S, Comina C, Boiero D, Socco LV (2009). Non-uniqueness in surface wave inversion and consequences on seismic site response analyses. Soil Dyn Earthq Eng 29(6), 982–993

Gallipoli, M.R., Mucciarelli, M., Eeri, M., Gallicchio, S., Tropeano, M., Lizza, C., (2004). Horizontal to Vertical Spectral Ratio (HVSR) measurements in the area damaged by the 2002 Molise, Italy. earthquake. Earthquake Spectra 20(1), 81-93, DOI: 10.1193/1.1766306.

Garofalo F., Foti S., Hollender F., Bard P.Y., Cornou C., Cox B.R., Ohrnberger M., Sicilia D., Asten M., Di Giulio G., Forbriger T., Guillier B., Hayashi K., Martin A., Matsushima S., Mercerat D., Poggi V. e Yamanaka H. (2016a) - InterPACIFIC project: Comparison of invasive and non-invasive methods for seismic site characterization. Part I: Intra-comparison of surface wave methods, Soil Dynamics and Earthquake Engineering, vol. 82, pp. 222-240, doi: 10.1016/j.soildyn.2015.12.010i.

Garofalo F., Foti S., Hollender F., Bard P.Y., Cornou C., Cox B.R., Dechamp A., Ohrnberger M., Perron V., Sicilia D., Teague D. e Vergniault C. (2016b) - InterPACIFIC project: Comparison of invasive and non-invasive methods for seismic site characterization. Part II: Inter-comparison between surface wave and borehole methods, Soil Dynamics and Earthquake Engineering, vol. 82, pp. 241-254, doi:10.1016/j.soildyn.2015.12.009.

GeoMol Team (2015) - GeoMol – Assessing subsurface potentials of the Alpine Foreland Basins for sustainable planning and use of natural resources – Project Report, Augsburg, LfU, p. 188 pp.

Guidoboni E., Ferrari G., Mariotti D., Comastri A., Tarabusi G., Sgattoni G., Valensise G. (2018) - CFTI5Med, Catalogo dei Forti Terremoti in Italia (461 a.C.-1997) e nell'area Mediterranea (760 a.C.-1500). Istituto Nazionale di Geofisica e Vulcanologia (INGV). http://storing.ingv.it/cfti/cfti5/

Gutenberg, B. (1958). Microseisms. Adv. Geophys., 5:53–92.

Herak, M. (2008). ModelHVSR-a Matlab tool to model horizontal-to-vertical spectral ratio of ambient noise. Comput. Geosci., 35:1514–1526.

Herak, M., Allegretti, I., Herak, D., Kuk, K., Kuk, V., Maric, K., Markusic, S., and Stipcevic, J. (2010). HVSR of ambient noise in Ston (Croatia): comparison with theoretical spectra and with the damage distribution after the 1996 Ston-Slano earthquake. Bull. Earthq. Eng., 8:483–499.

ISPRA (2009). Carta Geologica d'Italia alla scala 1:50.000, Foglio 203 Poggio Renatico. Coord. Scient.: U. Cibin, Regione Emilia-Romagna. ISPRA, Servizio Geologico d'Italia - Regione Emilia-Romagna, SGSS.

Kanai, K., Osada, T., and Tanaka, T. (1954). Measurement of the microtremors. Bull. Earthq. Res Inst., 32:199–209.

Konno, K. and Ohmachi, T. (1998). Ground-motion characteristics estimated from spectral ratio between horizontal and vertical components of microtremor. BSSA, 88(1):228–241.

Lacoss, R. T., Kelly, E. J., and Nafi, T. M. (1969). Estimation of seismic noise structure using arrays. Geophys., 34(1):21–38.

Lai, C. G., Foti, S., Godio, A., Rix, G. J., Sambuelli, L., and Socco, L.V. (2000). Caratterizzazione geotecnica dei terreni mediante l'uso di tecniche geofisiche. Rivista Italiana di Geotecnica, 34(3):99–118.

Laurenzano, G., Priolo, E., Barnaba, C., Gallipoli, M. R., Klin, P., Mucciarelli, M., and Romanelli, M. (2013). Studio sismologico per la caratterizzazione della risposta sismica di sito ai fini della microzonazione sismica di alcuni comuni della regione Emilia-Romagna - Relazione sulla attività svolta. Rel. OGS 2013/74 Sez. CRS 26, 31 luglio.

Louie, J.N. (2001). Faster, Better: Shear-Wave Velocity to 100 Meters Depth From Refraction microtremor arrays. BSSA, vol. 91, no. 2 (April):347-364.

Mantovani, A., Valkaniotis, S., Rapti, D., and Caputo, R. (2018). Mapping the palaeo-Piniada Valley, Central Greece, based on systematic microtremor analyses. *Pure Appl. Geophys.*, **175**, 865-881, doi: 10.1007/s00024-017-1731-7.

Margheriti, L., Azzara, R., Cocco, M., Delladio, A., and Nardi, A. (2000). Analyses of borehole broadband recordings: test site in the Po basin, Northern Italy. BSSA, 90:1454–1463.

Martelli, L. and Romani, M. (2013). Microzonazione Sismica e analisi della Condizione Limite per l'Emergenza delle aree epicentrali dei terremoti della pianura emiliana di maggio-giugno 2012 (Ordinanza del Commissario Delegato - Presidente della Regione Emilia-Romagna n. 70/2012) - Relazione illustrativa. http://ambiente.regione.emilia-romagna.it/geologia/temi/sismica/speciale-terremoto/sisma-2012-ordinanza-70-13-11-2012-cartografia.

Massolino, G., Abu Zeid, N., Bignardi, S., Gallipoli, M. R., Stabile, T. A., Rebez, A., Mucciarelli, M. 2018, Ambient Vibration Tests on a Building Before and After the 2012 Emilia (Italy) Earthquake, and After Seismic Retrofitting, 16th European Conference on Earthquake Engineering (16ECEE) June 2018, Thessaloniki, Greece.

Minarelli L., Amoroso S., Tarabusi G., Stefani M. and Pulelli G. (2016). Down-hole geophysical characterization of middle-upper Quaternary sequences in the Apennine Foredeep, Mirabello, Italy, Annals of Geophysics, vol. 59, no. 5, doi: 10.4401/ag-7114.

Molinari, F., Boldrini, G., Severi, P., Duroni, G., Rapti-Caputo, D., and Martinelli, G. (2007). Risorse idriche sotterranee della Provincia di Ferrara. Regione Emilia-Romagna (DB MAP Eds.). Florence, 61 pp.

Nakamura, Y. (1989). A method for dynamic characteristics estimation of subsurface using microtremor on the ground surface. Quarterly Report of RTRI, 30:25–33.

Nardon, S., Marzorati, D., Bernasconi, A., Cornini, S., Gonfalini, M., Romano, A., and Terdich, P. (1991). Fractured carbonate reservoir characterisation and modelling: a multisciplinary case study from the Cavone oil field. Italy, First Break, 9, 12, 553-565.

Nogoshi M., and Igarashi T. (1970) - On the propagation characteristics of microtremors., J. Seism. Soc. Japan, 23, 264-280.

Obradovic, M., Abu Zeid, N., Bignardi, S., Bolognesi, M., Peresani, M., Russo, P., Santarato, G., (2015). High resolution geophysical and topographical surveys for the characterization of Fumane Cave Prehistoric Site, Italy, Near Surface Geoscience 2015, DOI, 10.3997/2214-4609.201413676.

Ohori, M., Nobata, A., and Wakamatsu, K. (2002). A comparison of ESAC and FK methods of estimating phase velocity using arbitrarily shaped microtremor arrays. BSSA, 92(6):2323–2332.

Okada, H. (1986). A research on long period microtremor array observations and their time and spatial characteristics as probabilistic process. Report of a Grant-in-Aid for Co-operative Research (A) No. 59340026 supported by the Scientific Research Fund in 1985.

Okada, H. (2003). The Microtremor Survey Method. Geophys. Monograph Series, SEG, 129 pp.

Paolucci E., Albarello D., D'Amico S., Lunidei E., Martelli L., Mucciarelli M. and Pileggi D. (2015). A large scale ambient vibration survey in the area damaged by May–June 2012 seismic sequence in Emilia Romagna, Italy. Bulletin of Earthquake Engineering, 13 (11) pp. 3187-3206.

Park, C., Miller, R., and Xia, J. 1999. Multichannel analysis of surface waves. Geophysics, 64: 800-808.

Picotti, V. and Pazzaglia, F. (2008). A new active tectonic model for the construction of the Northern Apennines mountain front near Bologna (Italy). J. Geophys. Res., 113(B8).

Pieri, M. and Groppi, G. (1981). Subsurface geological structure of the Po Plain, Italy. CNR, Prog. Final. Geodin., pubbl. n. 414, Napoli.

Pondrelli, S., Salimbeni, S., Perfetti, P., and Danecek, P. (2012). Quick regional centroid moment tensor solutions for the Emilia 2012 (northern Italy) seismic sequence. Ann. Geophys., 55(4):615–621.

Priolo E., Romanelli M., Barnaba C., Mucciarelli M., Laurenzano G., Dall'Olio L., Abu Zeid N., Caputo R., Santarato G., Vignola L., Lizza C. and Di Bartolomeo P. (2012): The Ferrara thrust earthquakes of May-June 2012: preliminary site response analysis at the sites of the OGS temporary network. *Ann. Geophysics*, **55**(4), 591-597, doi:10.4401/ag-6172.RER & ENI-AGIP (1998). Riserve idriche sotterranee della Regione Emila-Romagna. A cura di G. Di Dio. S.EL.CA. (Firenze).

Ricci Lucchi, F. (1986). Oligocene to Recent foreland basins of northern Apennines. In Allen and P. Homewood (Eds.), Foreland Basins, volume 8, pages 105–139. IAS, Special Publication.

Rovida A., Locati M., Camassi R., Lolli B., Gasperini P. (eds), 2016. CPTI15, the 2015 version of the Parametric Catalogue of Italian Earthquakes. Istituto Nazionale di Geofisica e Vulcanologia. doi:http://doi.org/10.6092/INGV.IT-CPTI15

Scherbaum, F., Hinzen, K.G., Ohrnberger M., (2003). Determination of shallow shear wave velocity profiles in the Cologne/Germany area using ambient vibrations. Geophysical Journal International 152, 597-612.

Scrocca, D., Carminati, E., Doglioni, C., and Marcantoni, D. (2007). Slab retreat and active shortening along the Central-Northern Apennines. In Lacombe, O., Lavq, J., Roure, F., Verges, J. (Eds.), Thrust Belts and Foreland Basins: From Fold Kinematics to Hydrocarbon Systems, pages 471–487.

SESAME European project, 2004: Site Effects Assessment using Ambient Excitations; Deliverable D23.12: Guidelines for the implementation of the H/V spectral ratio technique on ambient vibrations: measurements, processing and interpretation; deliverable D13.08, Final report WP08, Nature of noise wavefield.

Tarabusi G. and Caputo R. (2016), The use of HVSR measurements for investigating buried tectonic structures: the Mirandola anticline, Northern Italy, as a case study, International Journal of Earth Sciences 106(1). doi: 10.1007/s00531-016-1322-3

Vannoli P., Burrato P. and Valensise G. (2014). The seismotectonics of the Po Plain (Northern Italy): tectonic diversity in a blind faulting domain, Pure Appl. Geophys., vol. 172, pp. 1105-1142, DOI: 10.1007/s00024-014-0873-0.

Tables

label	latitude	longitude	elevation [m asl]	distance along A-A'	distance from A-A'
ReMi009	4955137	680060	14.5	50	25
ESAC006	4957327	681804	13.0	2845	195
ReMi008	4958886	681953	11.3	4207	577
ESAC005	4959220	683215	12.6	5205	264
ESAC004	4960593	684254	12.6	6925	326
ESAC003	4961670	684477	12.5	7935	110
ReMi010	4962672	685739	11.9	9480	348
ESAC002	4963563	687038	12.0	10956	900
ESAC001	4965344	686964	11.1	12371	183
ESAC010	4966198	687706	10.0	13496	66
ReMi006	4966903	687298	10.4	13839	805
ESAC007	4967237	688560	10.3	14837	36
ReMi_BN14	4967683	688077	10.7	14925	615
ESAC008	4969316	690045	8.9	17392	58
ESAC011	4971209	691492	7.7	19773	155
ReMi_BN04	4972286	691344	8.7	20570	583
ESAC012	4972657	692754	8.2	21683	357
ESAC009	4973993	694016	7.6	23502	623
ReMi_BN11	4974513	694165	8.1	24013	447
ESAC013	4975738	694350	7.1	25122	104

Table 1: List of the array noise measurements along the Cento-Bondeno transect (see Figure 2a). Coordinate values refer to UTM zone 32.

label	latitude	longitude	elevation [m asl]	distance along A-A'	distance from A-A'
ESAC 01	4946530	714459	3.1	0	178
ESAC 02	4947330	715029	2.3	831	44
ESAC 03	4948470	715036	1.2	1883	483
ESAC 04	4949020	715811	1.3	2692	15
ESAC 05	4950090	716382	1.5	3900	122
ESAC 06	4950990	716572	0.5	4803	55
ESAC 07	4951940	716901	1.3	5805	123
ESAC 08	4952830	717258	1.2	6764	143
ESAC 09	4953800	717964	1.3	7933	127
ESAC 10	4954610	718249	3.9	8790	73
ESAC 11	4955510	718460	3.2	9700	84
ESAC 12	4956410	718774	4.4	10652	147
ESAC 13	4957680	719364	3.5	12052	100
ESAC 14	4958360	719532	2.0	12743	212
ESAC 15	4959510	720312	0.2	14107	56
ESAC 16	4960300	720546	0.2	14925	37
ESAC 17	4961180	720964	0.9	15898	3
ESAC 18	4962270	721064	2.8	16941	330
ESAC 19	4963050	721965	1.5	18011	193
ESAC 20	4963680	722199	0.9	18682	163
ESAC 21	4964950	722408	0.5	19933	141
ESAC 22	4965510	722620	0.2	20531	165
ESAC 23	4966480	723283	1.9	21683	66
ESAC 24	4967330	723543	2.4	22567	27
ESAC 25	4968010	723757	3.6	23277	96
ESAC 26	4969390	724651	2.2	24897	187

Table 2: List of the array noise measurements along the Traghetto-Formignana transect (see Figure 2b). Coordinate values refer to UTM zone 32.

label	latitude	longitude	elevation [m asl]	distance along A-A' [m]	distance from A-A' [m]	f_0 [Hz]	A_0	Vs [m/s]	inferred depth [m bsl]
site 01	4955190	680079	14.8	105	10	0.63 ± 0.08	2.5	280	96
site 02	4955730	680459	13.6	765	11	0.66 ± 0.09	2.6	272	95
site 04	4956600	680921	12.5	1742	110	0.58 ± 0.07	2.6	301	146
site 06	4957360	681481	14.0	2686	87	0.52 ± 0.03	3.1	295	138
site 07	4957870	681826	12.9	3302	98	0.60 ± 0.01	2.4	313	123
site 11	4959140	683232	12.3	5149	323	0.79 ± 0.04	2.8	330	107
site 15	4960850	684062	11.7	7026	21	0.69 ± 0.09	3.1	299	113
site 20	4963560	686137	11.1	10436	164	0.64 ± 0.03	3.1	237	98
site 22	4964940	686688	11.2	11882	177	0.64 ± 0.03	2.9	242	103
site 24	4965810	687340	10.2	12969	143	0.75 ± 0.16	3.5	292	104
site 25	4966888	688273	11.2	14387	2	0.73 ± 0.05	2.7	319	111
site 26	4967260	688551	10.0	14851	15	0.73 ± 0.09	2.7	321	112
site 28	4967920	689000	9.3	15649	4	0.73 ± 0.05	3.0	320	115
site 29	4969300	690001	9.0	17354	31	0.67 ± 0.16	2.5	348	122
site 30	4969700	690579	7.8	18013	275	0.66 ± 0.05	2.8	310	119
site 33	4971930	691579	8.5	20413	187	0.66 ± 0.04	2.9	292	102
site 34	4972230	691921	11.5	20855	80	0.70 ± 0.07	2.9	302	102
site 36	4974600	693686	8.3	23809	5	0.76 ± 0.08	3.5	304	116
site 37	4975040	694046	6.5	24376	47	0.72 ± 0.06	3.8	278	114
site 38	4975510	694174	7.2	24834	118	0.73 ± 0.11	3.7	279	113
site 39	4976030	694673	6.1	25547	8	0.78 ± 0.04	4.0	281	117

Table 3: List of the single-station noise measurements along the Cento-Bondeno transect (see Figure 2a). Coordinate values refer to UTM zone 32. All measurements lasted 30 minutes.

label	latitude	longitude	elevation [m asl]	distance along A-A' [m]	distance from A-A' [m]	f_0 [Hz]	A_0	Vs [m/s]	inferred depth [m bsl]
site 01	4946660	714455	2.5	0	314	0.79 ± 0.04	2.4	274	92
site 02	4947420	715103	2.5	937	16	0.84 ± 0.29	2.3	273	84
site 03	4948550	715112	1.1	2013	451	0.82 ± 0.02	2.4	288	82
site 04	4949120	715877	1.5	2805	31	0.82 ± 0.01	3.1	232	80
site 05	4950220	716457	1.5	4037	137	0.85 ± 0.09	2.3	261	78
site 06	4951100	716648	0.9	4928	32	0.66 ± 0.08	2.7	359	172
site 08	4952950	717359	1.0	6905	102	0.70 ± 0.06	2.1	278	73
site 09	4953830	718183	1.9	8038	311	0.58 ± 0.08	2.7	343	176
site 11	4955780	718605	3.4	9823	63	0.58 ± 0.02	2.5	360	179
site 13	4957780	719439	4.4	12164	77	0.79 ± 0.08	2.4	281	90
site 16	4960390	720624	0.2	15033	9	0.73 ± 0.03	2.7	304	103
site 17	4961300	721056	1.3	16027	37	0.73 ± 0.05	2.1	334	96
site 19	4963150	722025	1.4	18123	203	0.82 ± 0.13	2.2	290	85
site 20	4963770	722300	0.8	18803	212	0.70 ± 0.02	2.0	280	79
site 24	4967450	723634	2.2	22701	0	0.82 ± 0.08	2.2	324	115
site 26	4969500	724708	2.8	25007	187	0.78 ± 0.02	2.3	316	114

Table 4: List of the single-station noise measurements along the Traghetto-Formignana transect (see Figure 2b). Coordinate values refer to UTM zone 32. All measurements lasted 30 minutes except site 17 (46 min) and sites 24 and 26 (50 min).

Figure captions

Figure 1: Tectonic sketch map of the Ferrara Arc (from Pieri and Groppi, 1981) showing the location of the investigated profiles (A-A' and B-B').

Figure 2: Location of the array (yellow triangles) and single-station (blue squares) measurement sites along the a) Cento-Bondeno (A-A') and b) Traghetto-Formignana (B-B') transect. The background map represents the DTM from LIDAR survey.

Figure 3: a) Pseudo-2D shear-wave velocity section along the Cento-Bondeno transect. 1D velocity profiles from b) ESAC and c) Re.Mi. surveys. d) Location of the measured sites superimposed on the Structural Model of Italy (Bigi *et al.*, 1992).

Figure 4: Smoothed HVSR profile obtained by gridding each average HVSR curve, between 0.5 and 5 Hz. Relative amplitudes are color-coded (see colorbar). Some examples of the HVSR curves are also shown.

Figure 5: Example of HVSR inversion (site 39 along the Cento-Bondeno profile) with OpenHVSR routine (Bignardi *et al.*, 2016). a) Starting subsoil blocky layered model. b) Final subsoil blocky layered model. c) Best match between experimental and inverted data for the frequency range 0.5-5.0 Hz. d) Comparison between the smooth V_S models obtained from ESAC and HVSR inversions. e) Comparison between theoretical dispersion curve calculated for the final model and the experimental dispersion curve obtained from the analysis of the ESAC data recorded at the closest location.

Figure 6: a) V_S profiles obtained by the inversion of the HVSR curves, following the procedure discussed in the text. b) Particular of the geological profile (c) proposed by Martelli and Romani

(2013). AEI: Lower Emiliano-Romagnolo Subsynthem (Middle Pleistocene); AESind: undifferentiated Emiliano-Romagnolo Subsynthem (Middle Pleistocene); AES6: Bozzano Subsynthem (Middle Pleistocene); AES7: Villa Verrucchio Subsynthem (Late Pleistocene); AES8: Ravenna Susynthem (Late-Pleistocene-Present). The trace of the profile is represented in Figure 2b.

Figure 7: a) Pseudo-2D shear-wave velocity section along the Traghetto-Formignana transect. b) 1D velocity profiles from ESAC surveys. c) Location of the measured sites superimposed on the Structural Model of Italy (Bigi *et al.*, 1992).

Figure 8. a) Vs profiles obtained from the inversion of the HVSR curves, following the procedure discussed in the text. Portions of geological sections running from b) Montalbano to Consandolo (Molinari *et al.*, 2007), c) Cona to Maiero (ISPRA, 2009) and d) Baura to Tresigallo (Molinari *et al.*, 2007). Red stars represent the projection on the sections of the resonant interface(s) depth, inferred by HVSR curve inversion procedure, of the closest measured site. Units labels are reported in Figure 7, while the traces of the profiles are represented in Figure 2b.

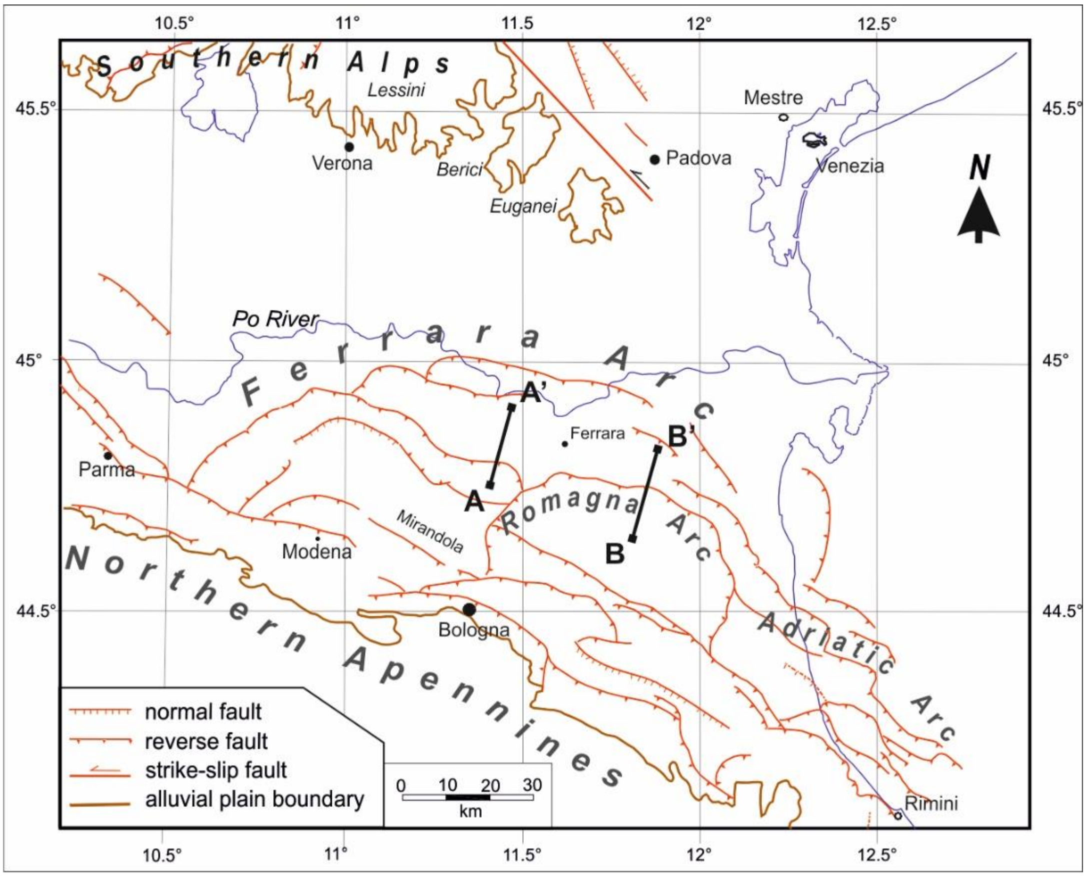

10.5°
11°
11.5
12°
12.5°
45.5°
45°
44.5°
S o u t h e r n A l p s
Lessini
Verona
Berici
Euganei
Padova
Mestre
Venezia
N
Po River
F e r r a r a A r c
A'
Ferrara
B'
Parma
A
Romagna Arc
Mirandola
Modena
B
N o r t h e r n A p e n n i n e s
Bologna
Adriatic Arc
Rimini
normal fault
reverse fault
strike-slip fault
alluvial plain boundary
0 10 20 30
km

Figure 1

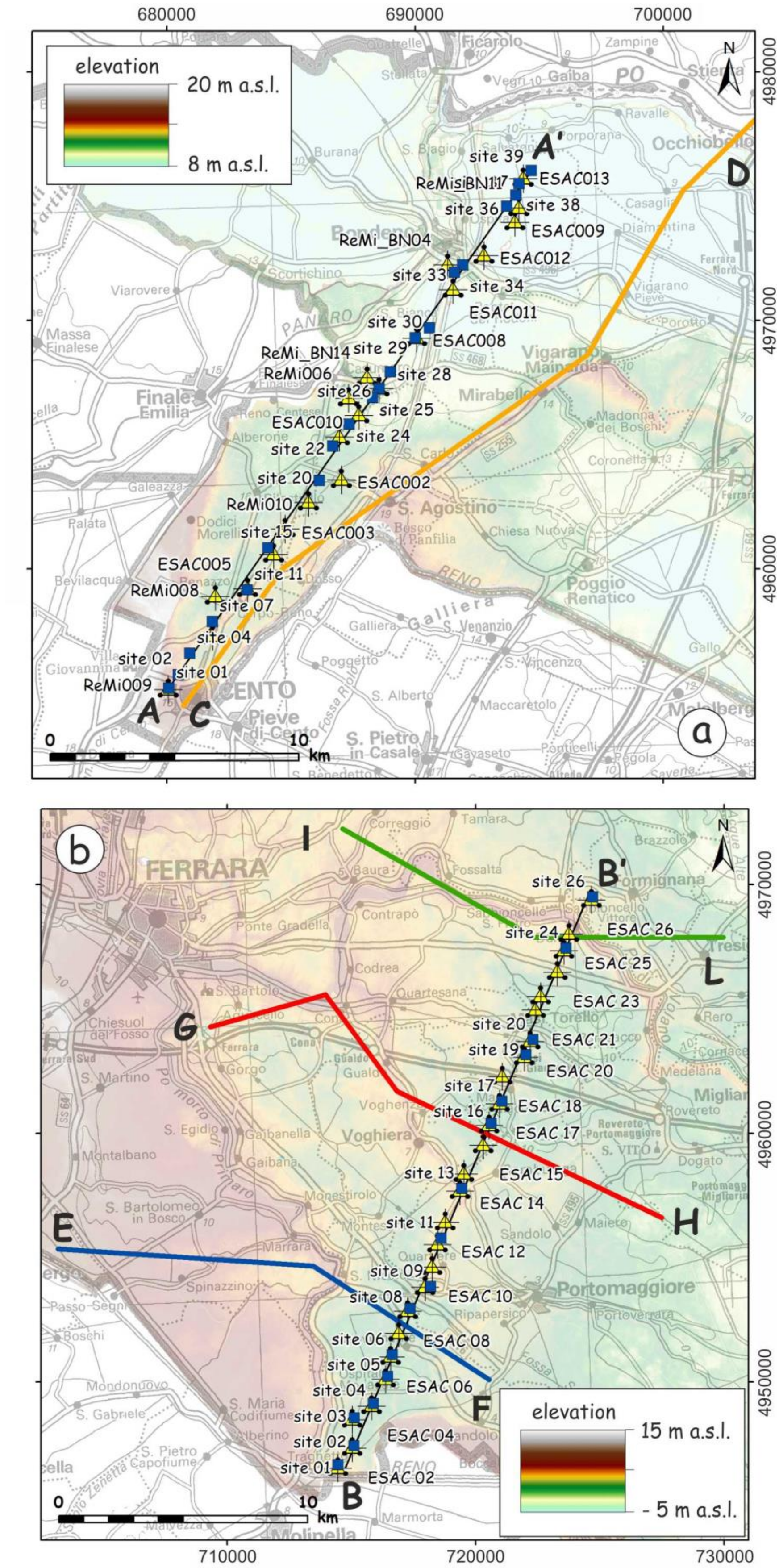
680000
690000
700000
4980000
4970000
4960000
elevation
20 m a.s.l.
8 m a.s.l.
A'
D
A
C
site 39
ESAC013
ReMisiBN11
site 36
site 38
ESAC009
ReMi_BN04
ESAC012
site 33
site 34
ESAC011
site 30
site 29
ESAC008
ReMi_BN14
ReMi006
site 28
site 26
site 25
ESAC010
site 24
site 22
site 20
ESAC002
ReMi010
site 15
ESAC003
ESAC005
site 11
ReMi008
site 07
site 04
site 02
site 01
ReMi009
0
10
km
a
b
FERRARA
I
B'
site 26
site 24
ESAC 26
L
ESAC 25
ESAC 23
G
site 20
ESAC 21
site 19
ESAC 20
site 17
ESAC 18
site 16
ESAC 17
site 13
ESAC 15
ESAC 14
H
E
site 11
ESAC 12
site 09
site 08
ESAC 10
site 06
ESAC 08
site 05
site 04
ESAC 06
F
site 03
site 02
ESAC 04
site 01
ESAC 02
B
elevation
15 m a.s.l.
- 5 m a.s.l.
710000
720000
730000
4950000

Figure 2

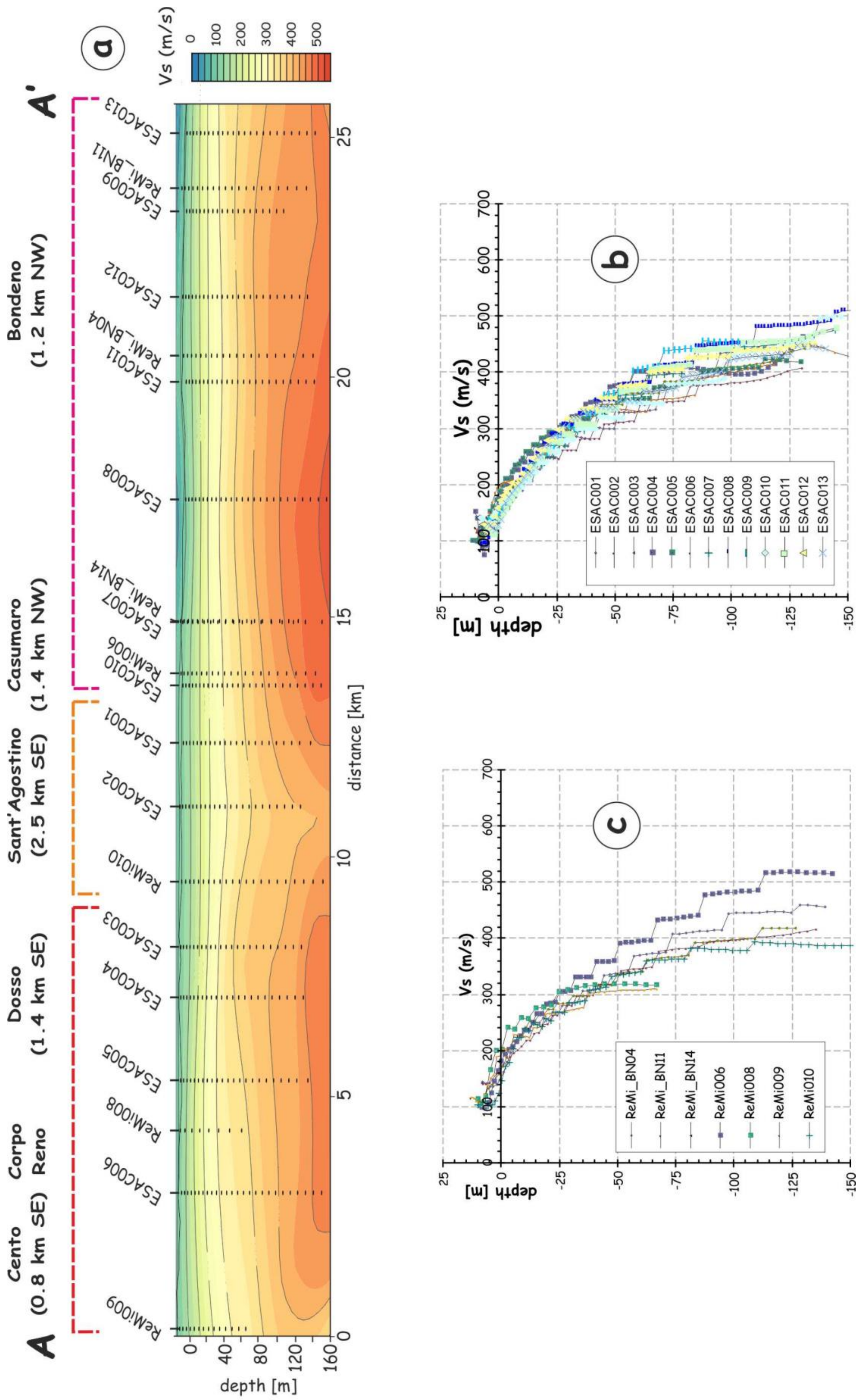

a
b
c
A
A'
Vs (m/s)
Cento (0.8 km SE)
Corpo Reno
Dosso (1.4 km SE)
Sant'Agostino (2.5 km SE)
Casumaro (1.4 km NW)
Bondeno (1.2 km NW)
ReMi009
ESAC006
ReMi008
ESAC005
ESAC004
ESAC003
ReMi010
ESAC002
ESAC001
ESAC010
ReMi006
ESAC007
ReMi_BN14
ESAC008
ESAC011
ReMi_BN04
ESAC012
ESAC009
ReMi_BN11
ESAC013
depth [m]
distance [km]
ESAC001
ESAC002
ESAC003
ESAC004
ESAC005
ESAC006
ESAC007
ESAC008
ESAC009
ESAC010
ESAC011
ESAC012
ESAC013
ReMi_BN04
ReMi_BN11
ReMi_BN14
ReMi006
ReMi008
ReMi009
ReMi010

Figure 3

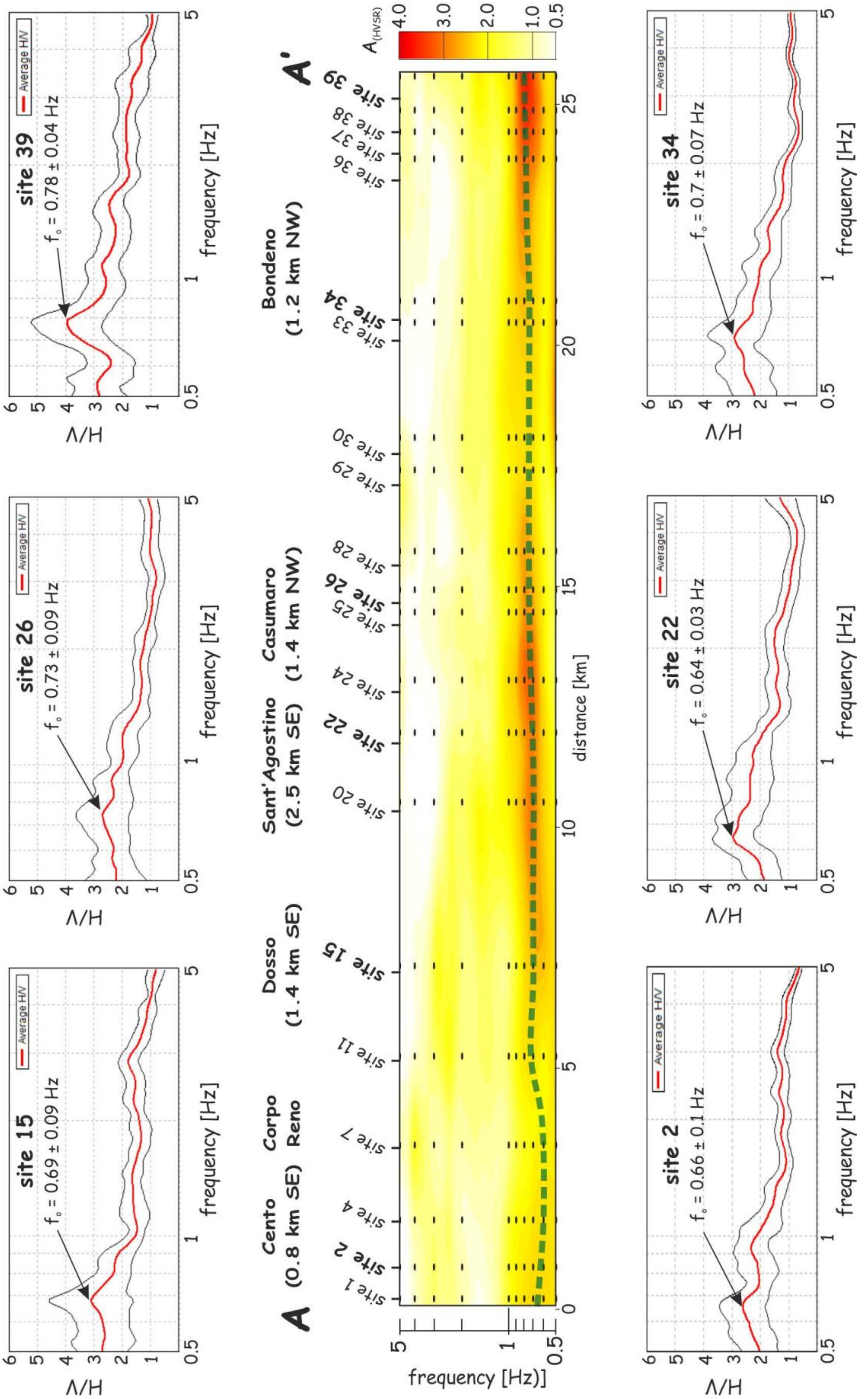

site 39
f_o = 0.78 ± 0.04 Hz
site 26
f_o = 0.73 ± 0.09 Hz
site 15
f_o = 0.69 ± 0.09 Hz
site 34
f_o = 0.7 ± 0.07 Hz
site 22
f_o = 0.64 ± 0.03 Hz
site 2
f_o = 0.66 ± 0.1 Hz
Average H/V
H/V
frequency [Hz]
A
A'
Cento (0.8 km SE)
Corpo Reno
Dosso (1.4 km SE)
Sant'Agostino (2.5 km SE)
Casumaro (1.4 km NW)
Bondeno (1.2 km NW)
distance [km]
frequency [Hz)]
$A_{(HVSR)}$

Figure 4

(a)

starting model

Vp [m/s]	Vs [m/s]	ρ [g/cm]	thickness [m]	Qp	Qs
1466.0	143.0	1.5	10.1	20.0	10.0
1543.0	211.0	1.5	9.4	40.0	10.0
1601.0	271.0	1.8	10.8	40.0	20.0
1650.0	324.0	1.9	19.7	40.0	20.0
1688.0	352.0	1.9	20.8	40.0	20.0
1715.0	382.0	1.9	21.1	40.0	20.0
1736.0	413.0	2.0	18.0	45.0	25.0
2000.0	800.0	2.1	999.0	999.0	999.0

(b)

final model

Vp [m/s]	Vs [m/s]	ρ [g/cm]	thickness [m]	Qp	Qs
1456.2	159.9	1.5	12.7	8.4	5.0
1532.3	212.8	1.5	9.9	9.3	5.0
1628.2	222.2	1.7	12.1	8.3	5.0
1639.9	274.3	1.8	19.4	30.8	19.4
1697.6	324.0	2.0	21.9	36.9	15.7
1740.9	410.7	2.0	20.7	40.2	24.3
1776.9	433.4	2.1	19.9	32.6	16.5
2000.0	600.0	2.1	999.0	999.0	999.0

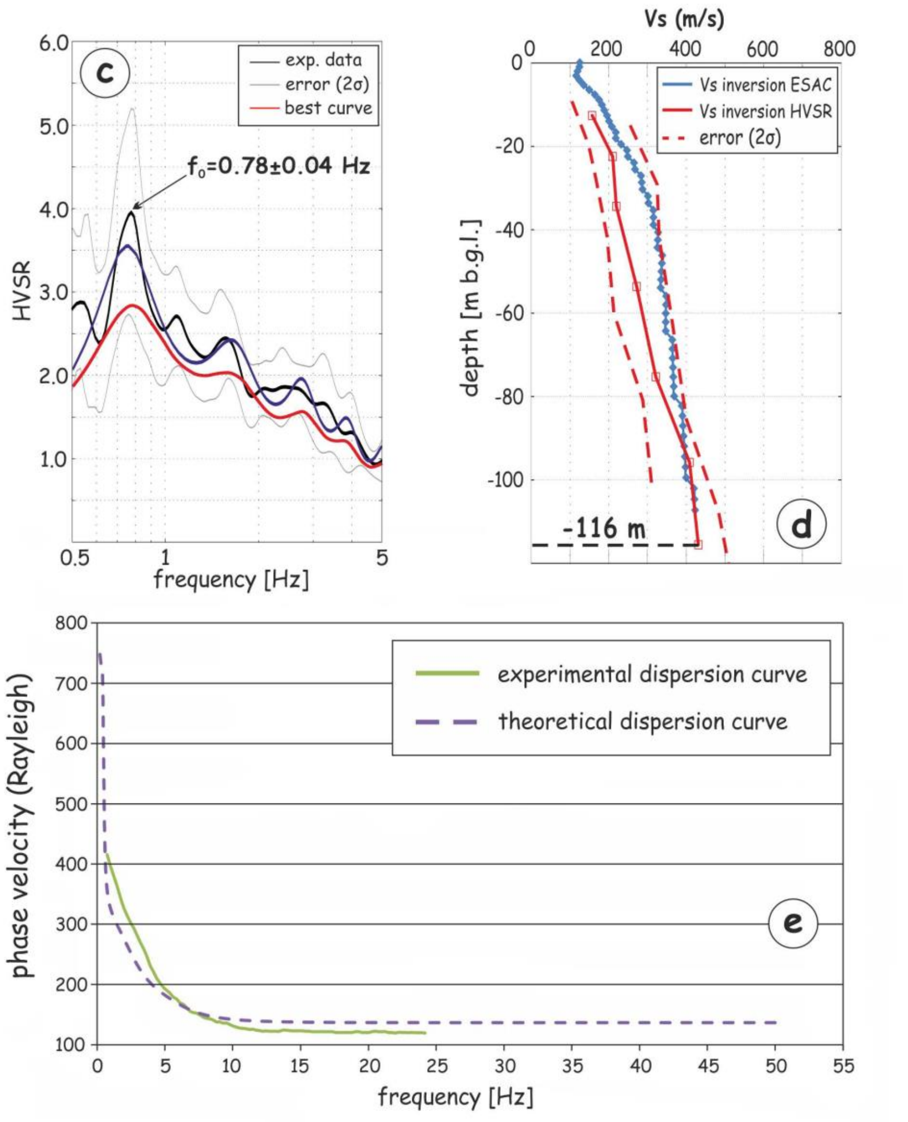

Figure 5

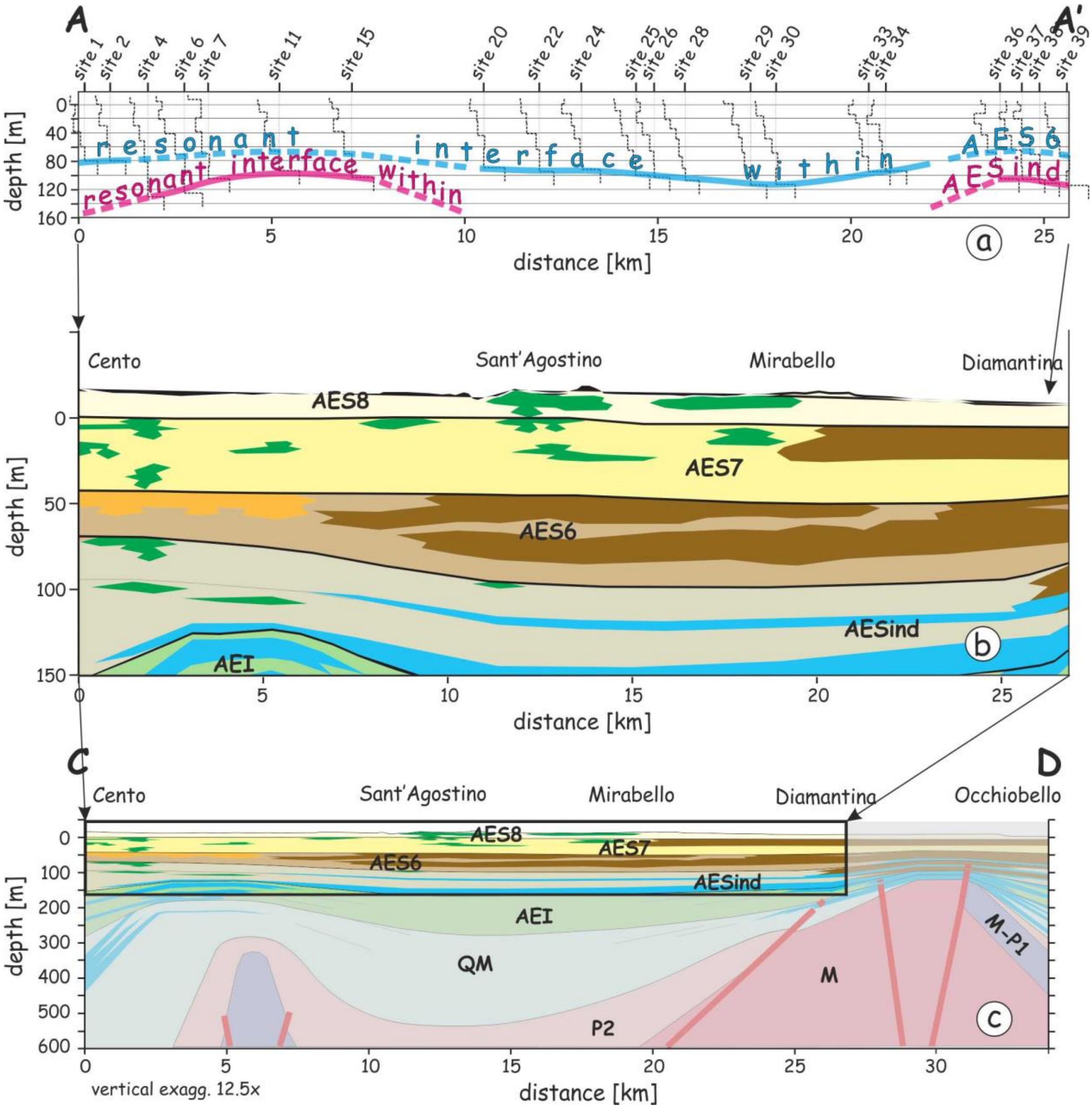
A
A'
site 1
site 2
site 4
site 6
site 7
site 11
site 15
site 20
site 22
site 24
site 25
site 26
site 28
site 29
site 30
site 33
site 34
site 36
site 37
site 39
depth [m]
resonant interface within AES6
resonant interface within AESind
distance [km]
a
Cento
Sant'Agostino
Mirabello
Diamantina
AES8
AES7
AES6
AESind
AEI
b
C
D
Occhiobello
QM
M
M-P1
P2
c
vertical exagg. 12.5x

Figure 6

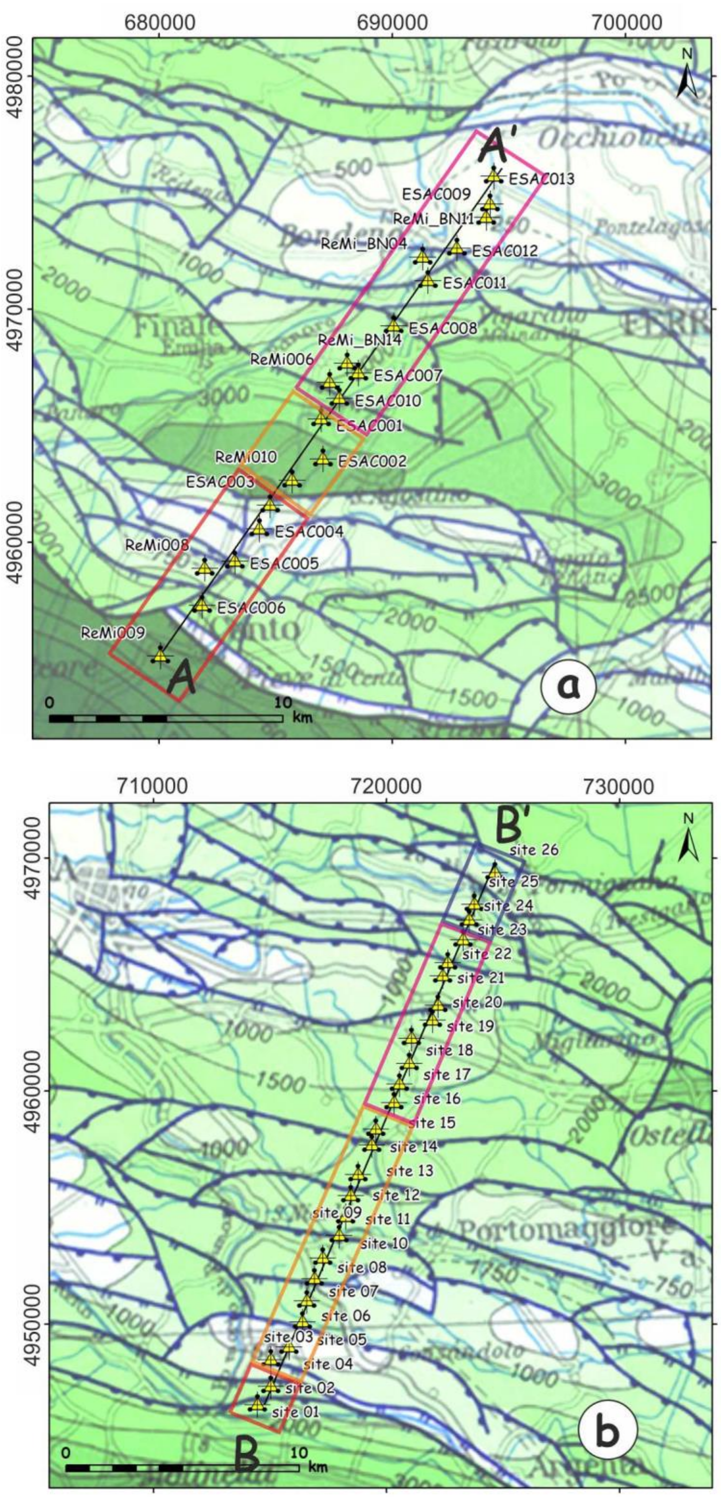
680000
690000
700000
4980000
4970000
4960000
A'
A
ESAC013
ESAC009
ReMi_BN11
ReMi_BN04
ESAC012
ESAC011
ESAC008
ReMi_BN14
ReMi006
ESAC007
ESAC010
ESAC001
ReMi010
ESAC002
ESAC003
ESAC004
ReMi008
ESAC005
ESAC006
ReMi009
0
10
km
a
710000
720000
730000
4970000
4960000
4950000
B'
B
site 26
site 25
site 24
site 23
site 22
site 21
site 20
site 19
site 18
site 17
site 16
site 15
site 14
site 13
site 12
site 09
site 11
site 10
site 08
site 07
site 06
site 03
site 05
site 04
site 02
site 01
0
10
km
b

Figure 7

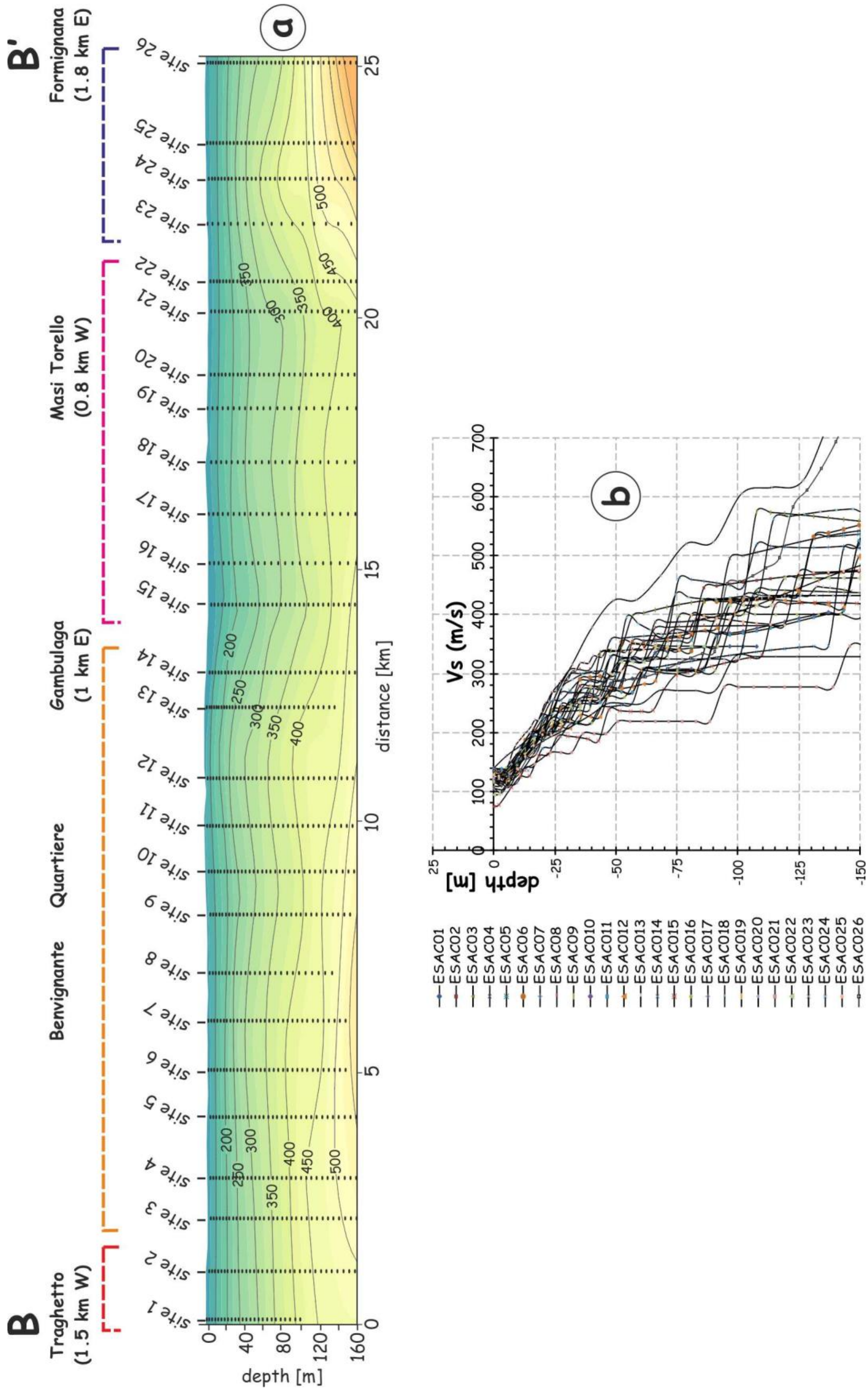
a
b
B
B'
Traghetto (1.5 km W)
Benvignante
Quartiere
Gambulaga (1 km E)
Masi Torello (0.8 km W)
Formignana (1.8 km E)
depth [m]
distance [km]
Vs (m/s)
depth [m]

Figure 8

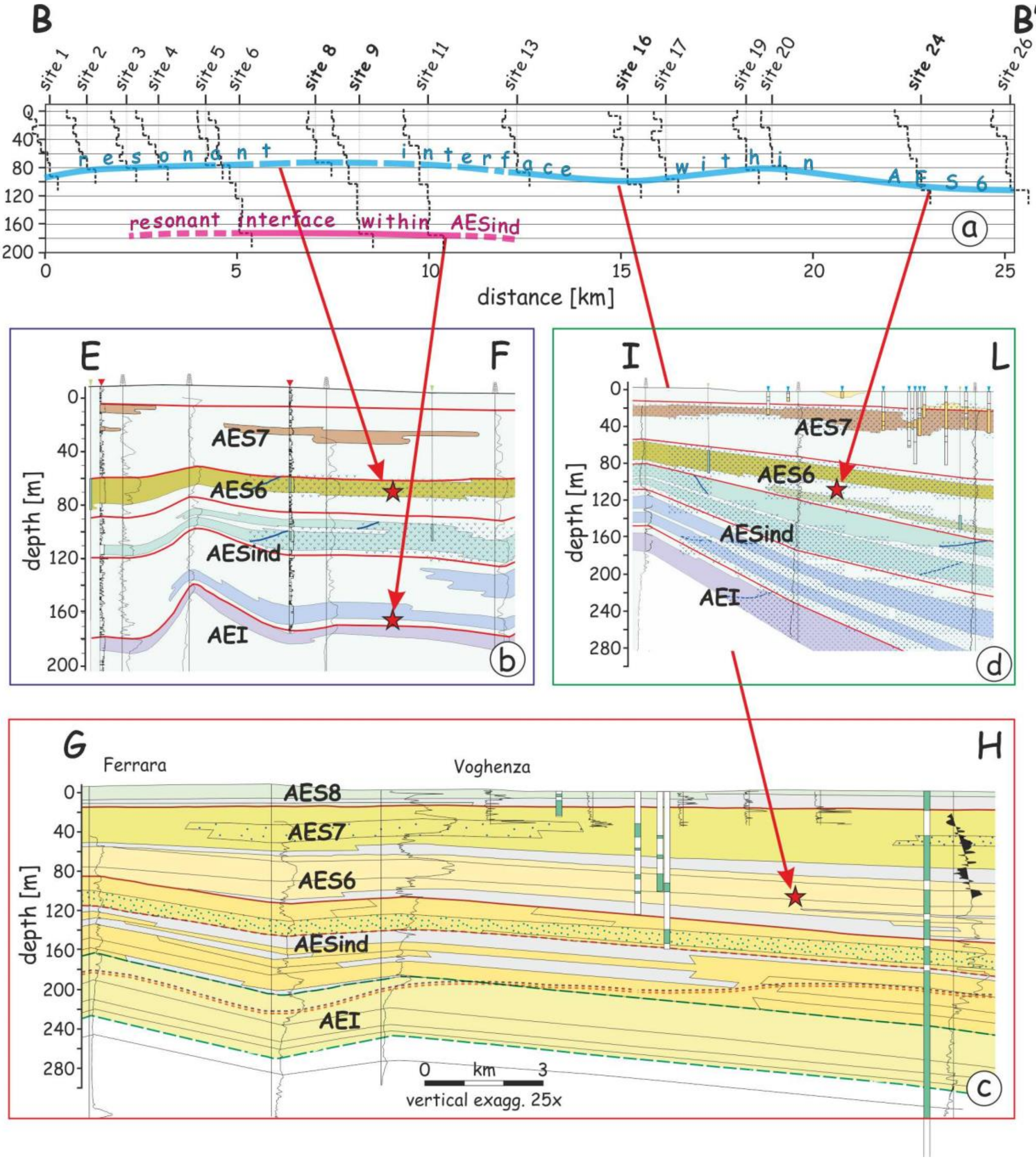
B
B'
site 1
site 2
site 3
site 4
site 5
site 6
site 8
site 9
site 11
site 13
site 16
site 17
site 19
site 20
site 24
site 26
depth [m]
resonant interface within AES6
resonant interface within AESind
distance [km]
a
E
F
AES7
AES6
AESind
AEI
b
I
L
AES7
AES6
AESind
AEI
d
G
H
Ferrara
Voghenza
AES8
AES7
AES6
AESind
AEI
0 km 3
vertical exagg. 25x
c

Figure 9